IEEE Access
Multidisciplinary | Rapid Review | Open Access Journal

Received 3 August 2022, accepted 15 August 2022, date of publication 18 August 2022, date of current version 26 August 2022.

Digital Object Identifier 10.1109/ACCESS.2022.3200058

SURVEY

Broken Bar Fault Detection and Diagnosis Techniques for Induction Motors and Drives: State of the Art

MOHAMED ESAM EL-DINE ATTA[1], (Member, IEEE), DOAA KHALIL IBRAHIM[2], (Senior Member, IEEE), AND MAHMOUD I. GILANY[2]

[1]Petroleum Pipelines Company, Mostorod, Kaliubia, Cairo 1104, Egypt
[2]Electrical Power Engineering Department, Faculty of Engineering, Cairo University, Giza, Cairo 12613, Egypt

Corresponding author: Doaa Khalil Ibrahim (doaakhalil73@eng.cu.edu.eg)

ABSTRACT Motors are the higher energy-conversion devices that consume around 40% of the global electrical generated energy. Induction motors are the most popular motor type due to their reliability, robustness, and low cost. Therefore, both condition monitoring and fault diagnosis of induction motor faults have motivated considerable research efforts. In this paper, a comprehensive review of the recent techniques proposed in the literature for broken bar faults detection and diagnosis is presented. This paper mainly investigates the fault detection methods in line-fed and inverter-fed motors proposed after 2015 and published in most relevant journals and conferences. The introduced review has deeply discussed the main features of the reported methods and compared them in many different aspects. Finally, the study has highlighted the main issues and the gaps that require more attention from researchers in this field.

INDEX TERMS Artificial intelligence, data-driven modeling, fault detection, fault diagnosis, frequency-domain analysis, induction motors, parameter estimation, signal processing, time-domain analysis, variable speed drives.

I. INTRODUCTION

Induction motors (IMs) are the most widespread electric motor type across a broad range of industries involving oil and gas, cement, petrochemicals, electric traction, etc., due to their robustness and low cost. In addition, this type of motor accounts for about 85% of the industrial sector's energy consumption [1]. Therefore, an effective fault detection and diagnosis (FDD) system becomes an inevitable requirement for the industry to avoid catastrophic unplanned shutdowns, minimize maintenance costs and reduce downtime.

Failures of IMs can be originated from faults in the stator, the rotor, the motor mechanical system including bearing and shaft, or external sources [2], [3]. Many surveys were conducted to estimate the percentage of failures related to each motor component. It was found that these percentages varied with motor size, application type, manufacturing standard,...etc. For example, medium voltage motors are more vulnerable to broken bar and end ring faults than small motors [2].

Rotor faults comprise both end ring and broken bar faults (BBFs). Examples of BBFs are shown in Fig. 1 and Fig. 2. These types of faults are mainly caused by one or a combination of the following reasons [4], [5], [6]:

- Dynamic stresses due to pulsating torques, concentrated centrifugal forces, and shaft torsional oscillation.
- Thermal stresses those caused by hot spots, overloads, sparking due to imperfect fabrication of the rotor, heavy and frequent starting, and plugging transients.
- Mechanical stresses caused by loose laminations, etc.
- Environmental stresses due to the contamination by chemicals.
- Magnetic stresses because of unbalanced electromagnetic forces.

Once a full BBF is introduced, the bar current that would flow in the broken bar transfers to the adjacent bars causing more thermal and magnetic stresses on these bars [7], [8], [9]. In addition, the backward magnetic field increases due to rotor circuit asymmetry which is reflected in the stator current harmonic content and other motor quantities [10]. Thus, the BBF reduces motor efficiency and reliability [3]. Also, the BBF causes the vibration of the shaft that may lead to bearing and rotor eccentricity faults [11]. As a consequence of these

The associate editor coordinating the review of this manuscript and approving it for publication was Gerard-Andre Capolino.

extra stresses, the adjacent bars and bearing become more susceptible to faults, the motor may not be able to develop the required torque, and eventually, a complete motor failure may occur [8], [9], [12], [13]. A sudden motor failure may cause severe consequences such as unplanned shutdown, loss of production, financial losses,...etc [3], [14]. Therefore, the early detection and diagnosis of BBFs become crucial to the modern industry.

A case of a complete rotor failure of a 380 kW, 6.6 kV motor is illustrated in Fig. 2. The rotor of this motor has 58 bars, 20 of them are damaged, so it could not deliver the required torque to drive the load which accounts for a complete rotor failure (based on the angle of the photo taken, only four broken bars are shown in Fig. 2).

FIGURE 1. Rotor of 460 kW, 6.6 kV motor with one broken bar marked with red color (the photo is taken by the authors).

In the last two decades, many review papers have attempted to analyze different FDD techniques of IMs and drives' faults in the literature such as [15], [16], [17], [18], [19], and [20]. However [15], [16], [19], and [20] provided broad reviews of FDD techniques of motor-drive systems including several electric machine types, faults types (BBF, stator faults, eccentricity, ...), and power electronics were provided. They discussed a limited number of researches related to BBF, perhaps due to the wideness of the review scope and the paper length limitations. Lastly, these references did not discuss methods proposed after 2015. Similarly, a comprehensive survey of FDD methods for the four major IM faults: broken bar faults, stator inter-turn faults, eccentricity faults, and bearing faults was provided in [17]. In this article, different FDD methods before 2016 were introduced and compared in several aspects. In contrast, and in an attempt to give more concern to IMs broken bar faults taking into account the paper length limitation, a more detailed review of detection and diagnosis methods before 2017 is achieved with mathematical representation in [18]. However, some significant points were not extensively reviewed concerning the detection of BBFs in inverter-fed IMs, diagnosis of non-adjacent BBFs in IMs, and also flux-based detection techniques. Additionally, the authors of [21] and [22] provided an overall comprehensive review of FFD for different devices and systems such as engines, motors, batteries,...etc. These two studies have proposed main frameworks for FDD techniques classification. A comparison with these seminal state-of-the-art papers is introduced in Table. 1.

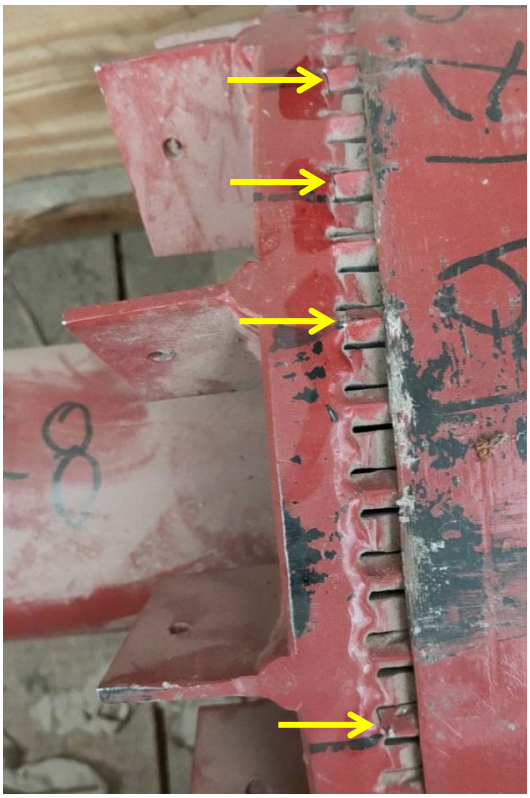

FIGURE 2. Rotor of 380 kW, 6.6 kV motor with multiple broken bars marked with yellow-colored arrows (the photo is taken by the authors).

So, this work is dedicated to filling the time gap between recent research studies and the latest available review articles and to help researchers to realize the current trends in this field (as shown in Table. 1). Also, the paper discusses the main BBF detection methods categories and considers the most common BBF signatures in the literature compared to other state-of-art and review papers. To enrich our review, integrate with previous works, and avoid duplications, most of the papers covered in this review were published after 2015 and more emphasis is placed on some highlighted points such as:

- Detection and diagnosis of BBFs in inverter-fed IMs.
- Classifying detection methods, including recent methods, into main groups and subgroups as demonstrated in Fig. 3 to help readers to comprehend the development of those methods.
- Holding extensive comparisons between different methods to show their merits and drawbacks.
- Assessing the usage of the data-driven approach in the detection and diagnosis of BBFs.

The rest of the paper is organized as follows: an overview of the nature of the BBF fault and the challenges that accompanied BBFs diagnosis are presented in Section II, and the

TABLE 1. A comparison between this article and most of the previous state-of-art and review articles.

	[15]	[16]	[17]	[18]	[19]	[20]	This article
Date of the covered research	Up to 2015	Up to 2015	Up to 2017	Up to 2018	Up to 2008	Up to 2014	Up to date
Machine of interest	Induction machines, synchronous machines, electrical drives, and power components and power converters	Induction machines, synchronous machines, electrical drives, and power components and power converters	Line-fed and inverter-fed squirrel-cage induction motors	Mainly Line-fed squirrel-cage induction motors	Line-fed and inverter-fed squirrel-cage induction motors	Induction machines, synchronous machines, electrical drives, and power components and power converters	Line-fed and inverter-fed squirrel-cage induction motors
Covered faults	Broken bar faults, inter-turn faults, bearing faults, and eccentricity	Broken bar faults, inter-turn faults, bearing faults, and eccentricity	Broken bar faults, inter-turn faults, bearing faults, and eccentricity	Broken bar faults	Broken bar faults, inter-turn faults, bearing faults, and eccentricity	Broken bar faults, inter-turn faults, bearing faults, and eccentricity	Broken bar faults including partial broken bars and non-adjacent broken bars under starting and steady-state conditions
BBF detection methods covered	• Time-frequency domain-based methods • Frequency-domain based methods • Data-driven based methods	• Frequency-domain based methods • Time-frequency domain-based methods • Time-domain based methods • Data-driven based methods	• Frequency-domain based methods • Time-frequency domain-based methods • Time-domain based methods • Data-driven based methods	• Frequency-domain based methods • Time-frequency domain-based methods • Data-driven based methods	• Resistance estimation-based methods • Parameter estimation-based methods • Frequency-domain based methods • Time-frequency domain-based methods • Time-domain based methods • Data-driven based methods	• Resistance estimation-based methods • Parameter estimation-based methods • Frequency-domain based methods • Time-frequency domain-based methods • Time-domain based methods • Data-driven based methods	• Resistance estimation-based methods • Parameter estimation-based methods • Digital twin-based method • Time-domain-based methods. • Frequency-domain based methods • Time-frequency domain-based methods • Data-driven based methods
Studied BBF signatures	Current signature	• Current signature • Flux signature	• Current signature • Flux signature • Vibration signature	• Current signature • Voltage signature • Vibration signature • Acoustic signature	• Current signature • Voltage signature • Flux signature	• Current signature • Flux signature	• Current signature • Voltage signature • Flux signature • Vibration signature • Acoustic signature

effect of BBF on motor variables is presented in Section III. Model-based methods are fully discussed in Section IV. Signal processing-based methods are reviewed comprehensively in Section V. Data-driven based methods are discussed in Section VI. Finally, the conclusions are drawn in Section VII in addition to some suggested future works.

II. MODELING OF BBF AND DIAGNOSIS CHALLENGES

In this section, the nature of the BBF and the diagnosis challenges will be discussed.

A. MODELING OF BBF

The broken bar fault is considered a type of asymmetry in the IM rotor circuit. This asymmetry results in increasing the backward magnetic field that already exists due to the inherent asymmetry of the rotor circuit [7], [12], [17]. The rotor's inherent asymmetry originates from the imperfection of the rotor casting, non-sinusoidal distribution of the rotor bars, etc. [7], [12], [23]. The increased backward field due to the fault deforms the motor magnetic flux density spatial

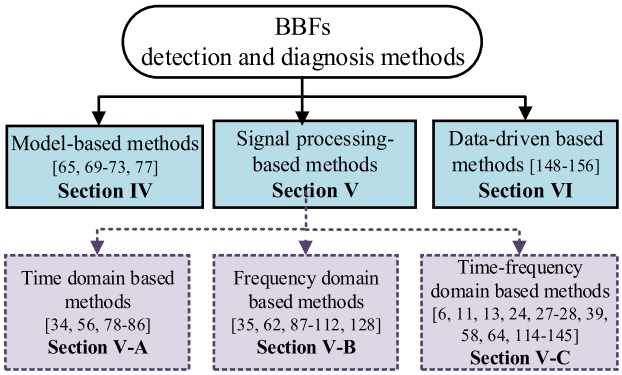

FIGURE 3. BBF detection and diagnosis methods classification.

distribution by creating undesirable highly saturated regions around the broken bar [7], [24].

A full broken bar can be modeled in the equivalent circuit by a virtual current source [7], [17]. The magnitude of this current source is equal to that of the current that would flow in the broken bar in the healthy case [7]. The current generated from this current source passes through the rotor bars adjacent to the broken bars besides their original current, causing more stress to these bars. This increase in the adjacent bars currents is because of the cancelation of the armature reaction created by the broken bar in the healthy condition [7], [13]. So, if the BBF is not diagnosed and cured early, the severity of the fault increases, and accordingly the rotor is susceptible to complete failure [12], [13].

It is worth mentioning that the partial broken bar can be represented as a less severe case of a full broken bar where a portion of the bar current can still flow because the connection is not fully broken as in the case of BBF [7].

B. CHALLENGES OF BBFs DIAGNOSIS

The types and modes of supply represent a major challenge for many fault detection and diagnosis methods. Therefore, in the next few lines, we will discuss different types of IM supply. These supply types can be classified into two main groups [7], [17]:

- Line-fed mode.
- Inverter-fed mode.

In the first type, the IM is energized by a constant-frequency sinusoidal voltage supply whereas, in the second type, the supply voltage fundamental frequency can be varied, and the voltage supplied to the IM is rich in harmonics [7], [17], [25], where these additional harmonics may mask the fault-related harmonics [25].

Also, in inverter-fed mode, many motor's mechanical and electrical variables are subject to continuous changes, while the variation in line-fed mode is mainly dependable on loading level [12]. Accordingly, the process of fault detection and diagnosis in inverter-fed mode represents a more sophisticated challenge.

Generally, the BBFs diagnosis challenges were discussed separately in several reported papers in the literature, however, these challenges will be briefly offered in the following points to provide a complete review of FDD.

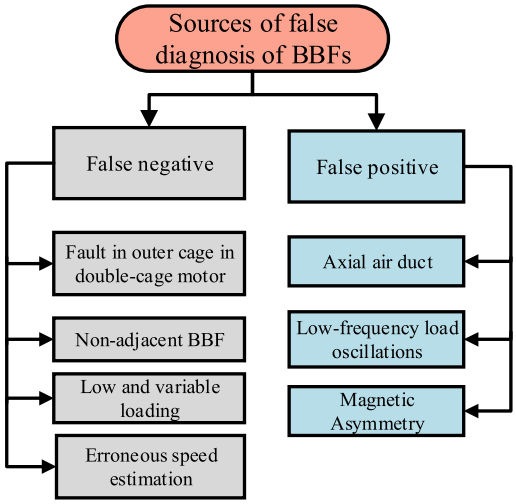

FIGURE 4. Classification of the sources of false diagnosis in the case of BBFs.

- The source of false diagnosis of BBFs can be classified into false positive and false negative sources as indicated in Fig. 4. Despite the high efficiency of many detection methods proposed in the literature, their accuracies may deteriorate under many motor designs, fault locations, and operating conditions [26], [27], 28].
- Related to motor design, the axial rotor air ducts are the most common cause of false detection of broken bars. Such ducts, which are used mainly for cooling, produce frequencies in the stator current spectrum similar to those induced in the case of BBFs [26], [27].
- A closed rotor slot is another obstacle related to motor design that undermines the performance of many fault detection methods [29].
- Besides, the non-adjacent broken bar is a typical fault location that is commonly misdiagnosed [30], [31].
- Also, a fault in the outer cage of a double cage motor can be hardly detected [28], [32].
- Erroneous speed estimation can lead to misdiagnosis for methods that require speed measurement.
- At the same time, the operating conditions and the mechanical load characteristics that negatively affect the FFD methods' accuracy include:
  - Low-frequency load oscillations [33], [34].
  - Light and zero loading conditions [18], [35].
  - Inverter-fed mode with closed-loop control strategies [36].
  - Short starting duration [13].

III. SIGNATURES OF BBF

Even though all motor variables are affected by BBF, some variables are more fault-sensitive [12]. These effects result in the appearance of certain patterns in the temporal evolution

of the signal, in its spectrum or its spectrogram. These patterns are widely known in the literature as fault signatures. Moreover, the measurement of some motor variables is more straightforward than others [12], [37]. In other words, the measurement requirements vary from simple non-invasive sensors with simple sampling techniques like current and voltage sensors to invasive sensors with especially sampling techniques like air-gap flux sensors [12]. Although air-gap flux sensors are the most reliable and fault-sensitive sensor types, current sensors are the most common to detect this fault due to their availability and ease of installation [12], [18], [38]. Therefore, there are two main trends:

- Increasing the reliability of the non-invasive methods through the development of post-processing techniques.
- Development of new non-invasive sensors that can measure more fault-sensitive motor variables.

An example of the first trend is the application of the dragon transform to a motor current signal to detect broken bar faults in an inverter-fed motor [38]. On the other hand, the usage of stray flux sensors represents the other trend [10].

Other fault signatures such as torque signatures do not attract researchers due to their low sensitivity and complexity [12].

In this paper current, voltage, flux, vibration, and acoustic signatures will be investigated.

A. BBF CURRENT SIGNATURE

As discussed in Section II.A, the BBF induces a backward magnetic field whose frequency equals sf_s and rotates in a reverse direction to the motor main flux, where s describes the motor slip and f_s is the supply frequency [7], [12]. This backward magnetic field finally develops a current component whose frequency equals $(1-2s)f_s$ [7], [12]. The new current component generates torque and speed ripples that generate another current component whose frequency equals $(1+2s)f_s$ [7]. The $(1+2s)f_s$ current component produces another $(1-4s)f_s$ component and the sequence continues [7]. More details and mathematical interpretation can found in [7] and [12].

Therefore, the characteristic frequencies of BBF f_{bbf} in the stator current are:

$$f_{bbf} = (1 \pm 2ks)f_s, \quad k = 1, 2, 3, \ldots \tag{1}$$

The fault-related harmonics can be recognized in the sideband around the supply frequency. The most significant fault-related harmonics for BBF detection in the literature are the first-order ones where $k = 1$ in equation (1). The sideband at $(1-2s)f_s$ is called left sideband harmonic (LSH) whereas, the sideband at $(1+2s)f_s$ is called right sideband harmonic (RSH). The magnitude and frequency of the LSH and RSH mainly depend on loading conditions, motor slip, load inertia, and the location of broken bars [39]. The effects of loading level and fault severity on the LSH and RSH in the motor current spectrum are shown in Fig. 5. Therefore, the detection of BBF under light and zero loading level using standard spectrum analysis methods would be impossible as the fundamental current component (FC) masks sideband harmonics at low slip as described by equation (1).

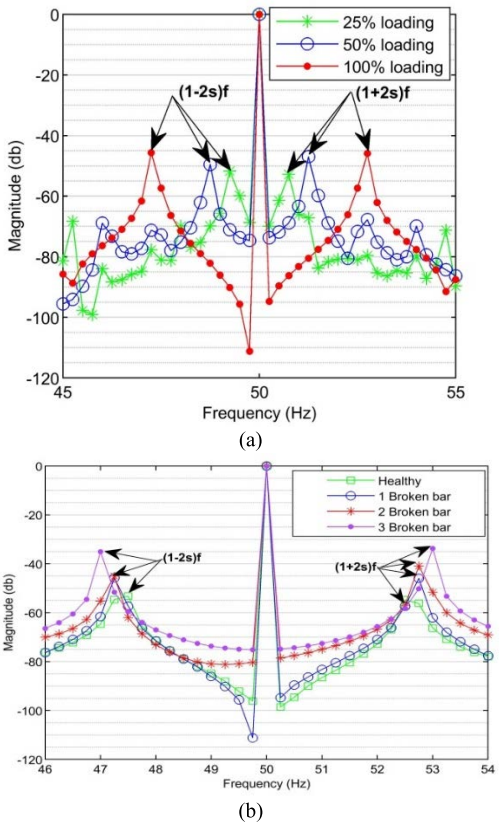

FIGURE 5. (a) Loading level effect and (b) fault severity effect Effects on LSH and RSH frequencies in the motor current spectrum (developed by authors and obtained by simulation test).

Based on Equation (1) and if we only consider the first-order sideband then, the stator current (I_a) can be expressed by:

$$\begin{aligned} I_a = {} & \sqrt{2}\, I cos\,(w_s t - \alpha) \\ & + \sqrt{2} I_l cos\,((1-2s)\, w_s t - \alpha_l) \\ & + \sqrt{2} I_r cos\,((1+2s)\, w_s t - \alpha_r) \end{aligned} \tag{2}$$

where I, I_l and I_r are the r.m.s of the FC, LSH, and RSH current components respectively. Whereas, α, α_l and α_r are the phase angles of the FC, LSH, and RSH current components respectively.

According to equation (2), the BBF induces periodic fluctuations into the stator current envelope in the time domain as shown in Fig. 6. Actually, as the fault severity increases, the amplitude of fluctuations increases [7].

In contrary to steady-state, the BBF detection under transient conditions is less sensitive to loading level and hence is more capable to detect such fault under zero loading conditions [13]. However, the BBF detection under transient conditions is influenced by load inertia since the inertia directly affects the starting time [13].

Nevertheless, the detection and diagnosis of BBF in inverter-fed induction motors are undisputed and more

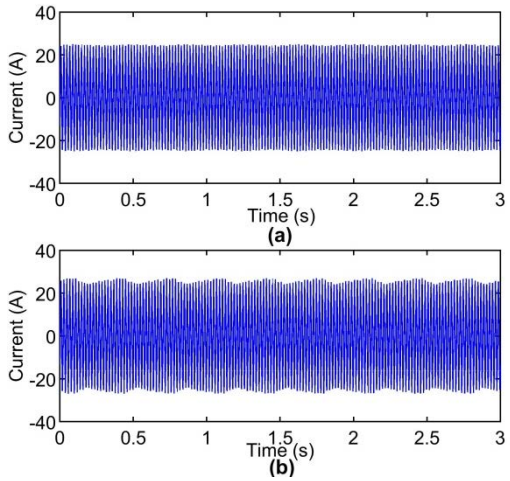

FIGURE 6. Steady-state stator current waveform in case of (a) Healthy motor and (b) motor with three broken bars (developed by authors and obtained by simulation test).

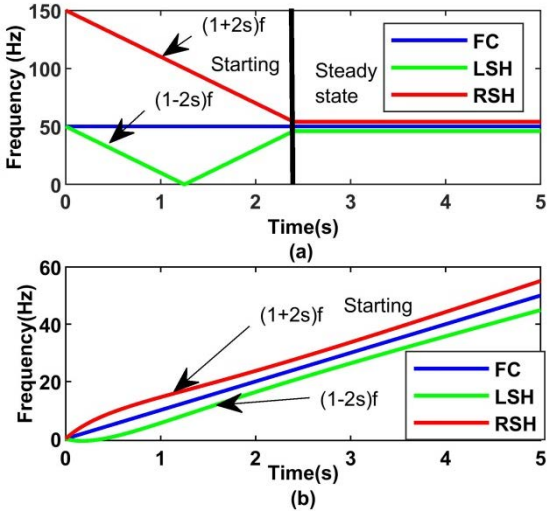

FIGURE 7. Theoretical trajectories of LSH and RSH of an induction motor in time-frequency plane (a) line-fed starting and (b) Inverter-fed starting (developed by authors and obtained by simulation test).

sophisticated in both steady-state and transient conditions since the high-frequency switching of the inverter produces several undesirable harmonics in the motor current and air gap flux [36].

In addition, the motor speed is no more dependable on the slip so, the BBF-related attributes are significantly different from those in line-fed cases [40]. The control strategies of the inverter have a great influence on sideband harmonics' magnitude and energy [36], [38]. The closed-loop control strategies such as field-oriented control system (FOC) and direct torque control (DTC) slightly increase the amplitudes of $(1 - 2ks)f_s$ [41], [42]. Whereas, the open-loop control strategies such as constant voltage/frequency (CV/F) significantly increase the main sideband frequencies [41].

As shown in Fig. 7, the LSH in line-fed mode has a unique V pattern in the time-frequency domain during motor starting that facilitates the detection of BBF. On the other hand, both the LSH and RSH are strictly close to the fundamental current component (FC) in the case of starting an inverter-fed motor. Consequently, the detection of BBF under these conditions is complicated.

Also, the BBF induces other frequency components around winding harmonics as expressed in [35]:

$$f_{bbf} = f_s\left(\left(\frac{k}{p}\right)(1-s) \pm 1\right), \quad {}^{k}/_{p} = 1, 3, 5, \ldots \tag{3}$$

where p is the number of pole pairs and k is an integer. This criterion was analyzed in steady-state and time-varying conditions in many papers to detect BBF such as in [43] and [44] when the diagnosis based on conventional harmonics LSH and RSH is not conclusive. The BBF occurrence increases the magnitude of many high-frequency components such as $(5 - 4s)f_s$ and $(7 - 6s)f_s$ [45]. These high-frequency current components are generated from the interaction of the spatial harmonics with the asymmetry due to broken bars.

As discussed in Section II.B, low-frequency load oscillations can induce frequencies in the stator current spectrum similar to that produced from the BBF [33], [34]. Many papers discussed this problem such as [34], [46], [47], [48], [49], and proposed different methods that can discern BBFs from load oscillations. These methods will be discussed later.

B. BBF VOLTAGE SIGNATURE

As discussed before, the BBF gives rise to asymmetrical rotor flux distribution. So, after disconnecting the main supply, the induced voltage in the motor stator winding reflects the rotor flux distortion [18]. Mainly the spectrum analysis of the induced voltage shows BBF-related components that can be used for fault detection and diagnosis [18]. The major drawback of this fault signature is that disconnection of the motor from the supply is required, which is not applicable in industrial applications. Besides, other faults such as stator winding faults induce fluctuations in the stator-induced voltage also [12].

Another BBF voltage signature is investigated in the literature to overcome the source disconnection requirement and provide continuous motor monitoring. It depends on measuring and analysis of the motor-neutral voltage that reveals fault-related information [50], [51]. The difficulty of measuring neutral voltage ranges from a simple connection in a star-connected winding motor to more advanced connections in the case of inverter-fed motors [51], [52]. In delta-connected winding motors, an alternative to the neutral voltage called stator circular current is used for fault detection and diagnosis [51]. However, the neutral-voltage signature provides one of the most accurate, robust, and reliable fault-related information for line-fed and inverter-fed motors [18].

In contrast to the effect of open and closed-loop control strategies on the current signature, the control strategies

have less effect on the voltage signature especially on zero-sequence voltage components [52].

C. BBF FLUX SIGNATURE

The motor air-gap flux is the coupling between the stator circuit and the rotor circuit, so any fault in the stator or the rotor appears in the air-gab flux. Hence, it is one of the most accurate and reliable motor fault-related signatures [28]. The BBF does not represent an exception to this rule; this fault increases the magnitude of flux density components whose frequencies depend on sf_s [53].

The variation of motor flux distribution due to BBF during starting is displayed in Fig. 8. The air-gap flux is measured using one search coil or more embedded in the air gap so, it is an invasive technique [28], [54]. Essentially, the induced voltage on the search coil is measured and analyzed to extract the fault signature. This fault signature can be used for fault detection in steady-state and starting conditions under line-fed and inverter-fed supply modes [12], [28]. This fault signature is immune from low-frequency load oscillations and unbalanced voltage supply [53].

To keep the advantages we got from air gap magnetic flux usage and avoid the invasive requirements for measuring air-gap flux, the motor stray flux is recently used in the literature. A coil or more is installed outside the motor in an axial or radial direction to capture the stray flux [10]. The BBF increases the magnitude of flux components in the axial direction whose frequencies equal sf_s and $3sf_s$ [28], [55]. It raises the magnitude of flux components in the radial direction whose frequencies equal $(5-4s)f_s$, $(5-6s)f_s$, $(7-6s)f_s$, $(7-8s)f_s$ [28], [55]. Then, the coil's induced voltage is analyzed to detect BBF [10], [28]. However, stray flux monitoring can provide nearly the same advantages as air-gap flux, the magnitude of the external stray flux is very low and depends on motor frame material [53], [56]. Moreover, a high-frequency resolution is required to distinguish the fault-related frequencies in the spectrum [53], [56]. Furthermore, the captured signal is susceptible to interference from other sources since the external search coil acts as a low-frequency antenna [53].

It is worth mentioning that the inverter control strategies have a considerable impact on the detectability of BBFs using stray flux. Generally, the inverter generates additional noise that may hide the fault-related frequency, especially at low slip [57]. Moreover, the compensation effect of the closed-loop control strategies suppresses some fault-related frequencies which makes the detection of such faults more challenging.

D. VIBRATION AND ACOUSTIC SIGNATURES

The vibration analysis is widely used for machines' health conditions monitoring. The vibration is generally produced by electrical, mechanical, and magnetic forces [18]. Based on the fact that the BBF results in unbalanced magnetic force conditions in addition to speed fluctuations [58], [59]. Therefore, vibration analysis can be used to detect such faults.

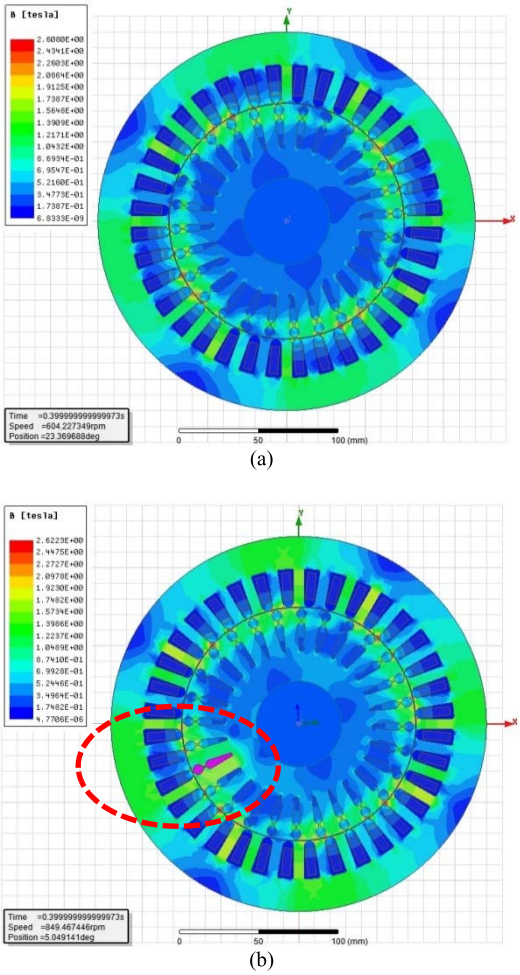

FIGURE 8. Magnetic flux distribution during starting of 11 kW IM (a) Healthy and (b) with one BBF (developed by authors and obtained by simulation test).

The vibration can be measured using different types of vibration sensors placed in axial or radial directions [58].

The spectrum analysis of vibration signals is usually used for fault detection purposes [58]. The BBF produces sideband harmonics around the rotational frequency [58], [59]. However, the detection methods based on vibration analysis were found experimentally to be more sensitive to bearing faults than BBF [58]. It is worth mentioning that the amplitude of the sideband harmonics depends on motor speed more than loading conditions [18], [58]. The inverter control strategies -especially closed-loop control such as FOC- have minor effects on the vibration signature [60]. However, the detection of BBF using vibration signature may require more advanced signal processing tools under low load operation conditions and variable loading conditions [60].

On the other side, the acoustics-based methods are very attractive to researchers for machine fault diagnosis as they contain less noise and interference within the frequency band of interest [18], [58]. In addition, they are noninvasive techniques as the acoustic signatures are captured by using a set of microphones [58], [61]. The BBF appears in

TABLE 2. Fault frequency components for different fault signatures.

Signatures	Frequency of interest	Notes
Current	$(1 \mp 2s)f_s$	Fault main sideband frequency components
	$f_s\left(\left(\frac{k}{p}\right)(1-s) \pm s\right)$; $k/p = 1, 3, 5, \ldots$	Fault high-frequency components (sidebands of winding harmonics) [35, 63]
Flux	$(1 \mp 2s)f_s$	Fault frequencies in stray flux in the radial direction [64]
	sf_s *and* $3sf_s$	Fault frequencies in stray flux in the axial direction [64]
	$(k_{odd} \pm k(1-s)/p)f_s$	Fault frequencies in the air-gab flux [28, 50]
Voltage	$(3k_{odd} - (3k_{odd} - 1)s \pm 2ks)f_s$	Fault frequencies in the neutral voltage [50]
Vibration	$f_r \pm (f_s - f_r)p$	Fault low frequencies in the vibration signal (pole pass frequency) [65]
	$f_r N_r \pm 2f_s$	Fault high frequencies in the vibration signal (rotor bar pass frequency)[65]
Acoustics	$3f_s - 2sf_s$	The fault frequencies in the acoustic signal [61]
	$(1 \mp 2ks)f_s$	the side band harmonics in the acoustic signal[61]

s : Motor slip; f_s : supply frequency; k : an integer 1, 2, 3,..; p : number of motor poles pairs; N_r: number of rotor bars; k_{odd}= 1, 3, 5,..; f_r: rotation frequency (Rotor speed).

the frequency spectrum as sideband harmonics around the driving frequency [58]. Unfortunately, the acoustic spectra cannot demonstrate explicit differences between healthy and BBF cases. Consequently, the acoustics-based methods are considered the least sensitive methods to BBFs [58].

E. CONCLUSION AND DISCUSSION ON BBF SIGNATURES

In a conclusion to this section, the BBF causes variations in all motor quantities with different degrees. These variations are reflected in motor measures such as current, voltage, flux, vibration, and acoustics, known as fault signatures. Table 2 illustrates the frequencies of interest for BBF detection and diagnosis for different signatures.

The BBF signatures can be measured using invasive or non-invasive techniques and require different conditions. In Table 3, a comparison between different BBF signatures was held to illustrate the differences between these signatures.

The sensitivity of different signatures to BBF is divergent. For example, the sensitivity of the air-gap flux signature to the BBF is superior to that of other signatures, but measuring this quantity requires an invasive technique [12], [28], [54]. On the other hand, the current signature analysis is the most common technique in the literature for BBF due to its non-invasive nature and simplicity.

IV. MODEL-BASED-METHODS FOR BBF DETECTION AND DIAGNOSIS

As illustrated in Fig. 3, this section is dedicated to discussing the conceptual basis of the model-based approaches. Generally, in model-based approaches, the IM is modeled to simulate its real behavior. A schematic diagram of the observer-based failure detection is displayed in Fig. 9. The observer or the state estimator can use the process inputs to estimate measurement variables [62]. The residual between the measured values and the estimated ones is used to identify the error [62].

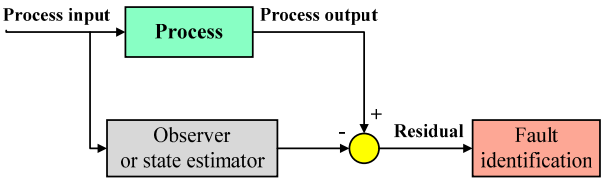

FIGURE 9. General scheme of the model-based fault methods [62].

There are three main approaches to these methods:

- Resistance estimation-based methods,
- Other parameter estimation-based methods,
- Digital twin-based methods.

The conceptual basis of the first approach is to use a state estimator to estimate the rotor resistance and compare it to a known value of rotor resistance for error detection. The deviation of the estimated resistance from a known value is used as an error severity indicator.

In contrast, the second approach estimates the parameter rather than the rotor resistance and compares it to the known value of the parameter. In this case, the severity of the error is assessed using these parameters. In general, this approach is suitable for mixed and simultaneous fault identification.

Finally, the digital twin technology offers a very promising tool for detecting BBF. This is because the technology can automatically estimate engine parameters and behavior based on online data.

A. RESISTANCE ESTIMATION-BASED METHODS

The problem of BBF detection for a sensorless vector-controlled induction motor drive was discussed in [66]. The used technique of control was based on the FOC in which the BBF effect in the speed is compensated. In this paper, the

TABLE 3. Comparison between different BBF signatures types.

Signature type		Invasive	Non-invasive	Online	Offline	Steady-state	Transient	Inverter-fed	Line-fed
Current		○	●	●	○	●	●	●	●
Voltage	Neutral voltage	○	●	●	○	●	NI	●	●
	Induced voltage	●	○	○	●	○	●	NI	●
Flux	Air-gap flux	●	○	●	○	●	●	●	●
	Stray flux	○	●	●	●	●	●	NI	●
Vibration		○	●	●	○	●	●	●	●
Acoustic		●	●	●	○	●	NI	NI	●

●: applicable; ○: not applicable; NI: not investigated.

extended Kalman filter (EKF) was used to estimate the speed of a sensorless vector control induction motor. In addition, EKF is applied to estimate in real-time the equivalent rotor resistance of the reduced multi-winding model of IM in healthy and faulty conditions under both transient and steady-state operation.

The estimated rotor resistance was proposed as a fault indicator. In addition, the spectrum analysis of stator current and quadratic current using fast Fourier transform was introduced for further confirmation of fault occurrence. The proposed method was validated experimentally as well as the results showed a good performance. Despite the effectiveness of the proposed method, 3-ph current and 3-ph voltage measurements besides motor parameters were required. Furthermore, EKF suffers from linearization error as well as the computational burden is high [67]. A comparative study between Unscented Kalman Filter (UKF) and EKF was introduced in [68] as promising methods to estimate the equivalent rotor resistance of the motor model. The two methods were tested using computer simulations under the same conditions. The test results illustrated that UKF had a better performance than EKF regarding computational burden, complexity, and mathematical stability. However, UKF may not converge in high-dimensional systems [67].

Later, Square–Root Transformed Cubature Quadrature Kalman Filter (SR–TCQKF) was proposed in [67] to overcome the EKF shortcomings, provide more accurate results, and ensure mathematical stability. The SR–TCQKF can accurately estimate the equivalent rotor resistance of the IM model. The change in the estimated rotor resistance from the reference value was utilized as a BBF fault indicator. This method was validated using a line-fed induction motor testbed under low loading conditions. The test results demonstrated that the proposed method precisely detected the BBF. Nevertheless, 3-ph current and 3-ph voltage measurements besides motor parameters were required.

B. OTHER PARAMETERS ESTIMATION-BASED METHODS

In [69], a model based on Park's model for BBF and stator inter-turn faults was developed for IMs. The faulty parameters were estimated using this model and sequential electrical data samples with the help of the output error technique to indicate fault level, while the other motor model parameters did not change. This method was validated using a set of experiments. Although this method showed very good accuracy and was suitable for inverter-fed IMs with FOC algorithms, 3-ph current, 3-ph voltage, and speed measurements besides motor parameters were required. These requirements may be not available in a real case.

Furthermore, the model-based approach was applied in [62] to detect incipient BBF and inter-turn faults. The dynamic nonlinear unknown input observer (DNUIO) was presented to overcome motor nonlinearity problems and load variations effects. The DNUIO was used to predict the rotor equivalent resistance of a highly nonlinear model of IM. This method was verified using simulations to illustrate its effectiveness and asymptotic stability. However, 3-ph current, flux, and speed measurements besides motor parameters were required.

On the other hand, an analytical model that can represent IM with stator inter-turn faults and BBFs occurring simultaneously or alone was presented in [70]. The proposed method can detect motor faults in real-time by utilizing the pendulous oscillation phenomenon of the magnetic field with the aid of particle swarm optimization. The experimental validation of the proposed method using a line-fed induction motor illustrated that the method is immune to load variations, voltage unbalance, and voltage distortion. Contrary, the proposed method is susceptible to false classification. Like the previous method, 3-ph current and 3-ph voltage measurements were required.

C. DIGITAL TWIN-BASED METHODS

Another trending technology is called digital twin (DT), which is the creating and sustaining of a digital representation of physical objects and supporting their performance through digital simulation and optimization tools that are continuously fed with real-time and updated data [71].

Normally, the digital twin architecture typically consists of five main components; the physical entity in the real world, the virtual entity, the services entity, the data, and the connections [71], [72]. The virtual entity simulates the physical object from different approaches and provides multi-functions for the digital twin such as fault identification, optimization, simulation, and control strategies [72]. The data drives the complete system and updates the digital model. The service entity acts as a platform with a variety of services. Also, it reacts to requests from both physical and

virtual entities [72]. The DT automatically measures and estimates motor parameters and quantities based on online data, which generally makes it a very efficient tool for detecting motor faults [72]. On the other hand, the DT faces many challenges such as developing comprehensive multi-physical modeling with a suitable calculation burden for online simulation, worthless complexity, expensive technology, etc. [72], [73].

The DT term was used in the field of broken bar fault detection only in [74], but in a way represents a misconception of definitions in [71] and [72]. In [74], a 3-D finite element model was introduced to simulate a 5-hp motor. The stator current obtained by the simulation was used to test artificial neural networks (ANN) accuracy to classify BBF.

D. DISCUSSION ON MODEL-BASED METHODS FOR BBF DETECTION AND DIAGNOSIS

To conduct some comparative analysis between different methods introduced in the literature, some abbreviations are used as defined in Table. 4. Accordingly, a detailed comparison among different model-based methods is illustrated in Table. 5.

It can be concluded that the model-based methods require a relatively large number of sensors and a detailed knowledge of motor models and parameters compared to other BBF detection methods. Also, a precise selection of the observer's type is essential for rigorous results in both resistance estimation and other parameter estimation-based methods. Furthermore, the rotor temperature estimation accuracy is largely dependent on the identification accuracy. However, most of these methods can provide accurate results under zero in addition to low loading conditions, unbalanced voltage supply, mixed faults, and closed-loop inverter fed modes which represent a stumbling block for most of the other methods.

The digital twin-based methods represent a trending technology for efficient monitoring and accurate fault detection and diagnosis of IMs. However, it may not be the best solution for monitoring small motors due to the cost of implementation and complexity. Nowadays, developing a multi-physical model for the IM with a compromised computational burden and accuracy for online simulations takes researchers' attention.

V. SIGNAL PROCESSING–BASED METHODS FOR BBF DETECTION AND DIAGNOSIS

The concept of these methods is to use a variety of different techniques to extract the fault-related features from the measured signals. These features can be extracted from the time, frequency, or time-frequency domain.

A. TIME-DOMAIN-BASED METHODS FOR BBF DETECTION AND DIAGNOSIS

In this subsection, FDD methods that are based on processing data obtained from the measured signals in the time domain are presented.

A straightforward algorithm to automatically detect BBFs even at the incipient phase under starting conditions was proposed in [75]. Firstly, the starting current signal was filtered and segmented before being processed. In the processing stage, the segmented current was compared with a set of reference current signals that represent healthy and different fault conditions. This algorithm can efficiently diagnose the BBF however, reference current signals were required.

A method based on the spectral analysis of the air gap flux measured by a hall effect sensor embedded between two stator slots was proposed in [76] to diagnose BBF in IMs running at very low slips. In this method, multiple statistical features were extracted from the time domain and frequency domain of the air-gap flux to be fed to different artificial intelligence classifiers for BBF detection and classification. However, an invasive technique was used to measure the air gap flux and large data was used to train the classifier.

TABLE 4. Abbreviations used in Tables 5, 6, 7, 8, and 9.

A: Acoustic sensor	I/NI: Invasive/Non-invasive
C: Current sensor	S/T: Steady-state/Transient
V: Voltage sensor	On/Off: Online/Offline
S: Speed sensor	L/IN: Line-fed/Inverter-feed mode
F: Flux sensor	Exp/Sim: Experimental/Simulation
VS: Vibration sensor	N/A: Not Applicable
BRB: Broken rotor bar	U/K: Unknown

In contrast, in [77], the information entropy analysis of the current waveform at either starting or steady-state was utilized as an index for BBFs. Although the low complexity and the high efficiency of the proposed method under starting and steady-state, several trials were required to determine the thresholds in a process similar to the training process.

The investigation of vibration and current monitoring for effective mechanical and electrical fault prediction in IMs was introduced in [78]. Three statistical features extracted from current and/or vibration in the time domain were employed in [78] in conjunction with a multiclass support vector machine to detect BBFs in addition to different electrical and mechanical faults. The proposed scheme was validated experimentally. The test results showed that a high accuracy could be achieved using the current signal only. Another objective of this paper was to hold a comparison between vibration signal and current signal as a media for detecting different electrical and mechanical faults. It was found that the vibration signal and current signal provided information-rich media for detecting mechanical and electrical faults respectively however, both signals were required for efficient detection of combined mechanical and electrical faults.

On the other hand, an invasive method was presented in [79] that was based on a differential measurement of the air-gap magnetic field captured by two series search coils installed on the stator tooth. The resultant induced voltage at the series coils terminals was employed as a fault indicator.

TABLE 5. Comparison among different model-based methods discussed in Section IV.

[Reference] (year)	Number-sensor type	L/IN	I/NI	S/T	On/off	Type of validation	Fault severity	Fault indicator
[66] (2017)	3-C, 3-V	IN	NI	S &T	On	Exp. &Sim.	2 BRB	Rotor resistance estimation and FFT of stator current
[67] (2019)	3-C, 3-V	L	NI	S &T	Off	Exp. &Sim.	1&2 BRB	Rotor resistance estimation
[68] (2010)	3-C, 3-V, 1-S	L	NI	S	On	Sim.	1&2 BRB	Rotor resistance estimation
[62] (2015)	3-C, 1-F, 1-S*	L	I	S	On*	Sim.	2 BRB	Residual between measured and estimated current, flux, and speed values
[69] (2006)	3-C, 3-V, 1-S	IN	NI	S	Off	Exp.	1&2 BRB	Fault parameter estimation
[70] (2019)	3-C, 3-V	L	NI	S	On	Exp. &Sim.	1&2 BRB	the pendulous oscillation of the magnetic field with the aid of particle swarm optimization
[74] (2021)	3-C	L	NI	S	Off*	Sim.	2 BRB	N/A

*: as inferred by authors.

Later in [80], a method is introduced that could effectively discriminate both BBF and eccentricity fault and then estimate the severity of each fault. In this method, the air-gap flux density was acquired using 36 flux sensors installed in the air gap. The analysis of the air-gap flux density in both time and space was the base of BBF detection and diagnosis in that study.

Furthermore, the homogeneity of one phase stator current during the starting was suggested in [81] to be used for early detection of BBF with a relatively low computational burden. The proposed method was experimentally validated as an online tool that can detect and classify BBFs even in the early stages. This method could achieve a high accuracy reaching 99.7%, however, a considerable amount of data was required to define acceptance and rejection regions. Although the proposed method successfully diagnosed faults of different levels of severity up to two broken bars, we think that diagnosing faults of higher severity will be challenging for this method. As with the increase of the fault severity over two broken bars, the density function of the homogeneity in the case of fault resembles that in the healthy cases.

The orthogonal Component Decomposition technique (OCD) was utilized to efficiently detect BBF in both line-fed and inverter-fed modes in [82]. It was found that the decomposition products of currents and voltages are rich in fault-related data in both the two operation modes. The proposed technique is supported by support vector machines to detect and classify faults with accuracy that reached 100% and 98.76% in the case of line-fed and inverter-fed modes respectively.

The differential measurement of the air-gap magnetic field was employed again in [53] to detect BBF even under load torque oscillations, unbalanced voltage source, and non-adjacent BBF. The time-domain analysis of the differential induced voltage at two search coils per phase was introduced as a fault indicator.

The chaos theory-based method was proposed in [83] as a prospective solution to detect and classify BBF under low slip conditions and variable loading conditions with the minimum window length. The analysis of only one chaotic variable called density of maxima could efficiently indicate BBF occurrence.

A Histogram of Oriented Gradients (HOG), a widely used image-processing tool, is used in [33] to detect the BBF of an IM running at low slip conditions without the need for slip measurement. The HOG extracted features were fed to a multilayer perceptron neural network and Bayesian classifier for fault detection and classification. The proposed method was validated under no-load conditions and in the existence of oscillatory loads.

Finally, a detailed comparison among different time-domain-based fault detection methods introduced in the literature is presented in Table. 6.

B. FREQUENCY-DOMAIN-BASED METHODS FOR BBF DETECTION AND DIAGNOSIS

In these methods, various signal processing techniques are applied to extract fault-related features from the signals in the frequency domain.

1) FAST FOURIER TRANSFORM-BASED METHODS

In these methods, the frequency spectrum of several quantities such as current, magnetic flux, power, etc. is used for fault detection. This frequency spectrum is calculated primarily using fast Fourier transform (FFT).

Motor current spectrum analysis using FFT is one of the most common and early techniques used to detect BBFs. However, the FFT is valid only for steady-state operation. Also, it suffers from several limitations like spectral leakage and low-frequency resolution. Therefore, different solutions were presented in the literature to overcome these limitations. In [84], to overcome the problem of detecting BBF in large IMs running at very low slip, the resultant magnetic flux density was analyzed instead of the current using FFT to avoid the high-frequency resolution requirement in the case of current spectrum analysis under low-slip operation, however, a special arrangement was required for the installation of the flux sensor. Furthermore, the air-gap and radial leakage flux were analyzed by FFT in [85], where the attenuation of the f_r sidebands component was used as a fault indicator. The aim of the proposed method was to overcome motor-current-signature analysis (MCSA) drawbacks and to discriminate BBF from other fault and load defects. In [34], the magnitude of certain frequencies in the frequency spectrum of the stray

TABLE 6. Comparison among different time-domain-based fault detection methods discussed in Section V-A.

[Reference] (year)	Number-sensor type	L/IN	I/NI	S/T	On/off	Type of validation	Fault severity	Loading (%)	Sampling frequency	Training (%)	Accuracy (%)
[75] (2018)	1-C	L	NI	S	On	Exp.	0.5, 1,2 BRB	U/K	1.5 kHz	25	100
[76] (2018)	1-F	L	I	S	Off*	Exp.	1, 2, 4 BRB	0-100	10 kHz	85.5*	Up to 100*
[77] (2021)	1-C	L	NI	S/T	Off*	Exp.	1BRB	25-100	1.5 kHz	U/K	95-99.7
[78] (2017)	3-VS	IN	NI	S	Off*	Exp.	U/K	0- high-load*	2 kHz	80	92.3
	3-C	IN	NI	S	Off*	Exp.	U/K	0- high-load*	2 kHz	80	87.5-92.5*
[79] (2017)	2-F	L&IN	I	S	On	Exp. &Sim.	1, 2, 5 BRB	U/K	U/K	N/A	U/K
[80] (2018)	36-F	IN	I	S	On*	Exp. &Sim.	0.5 BRB	20-80	U/K	N/A	U/K
[81] (2017)	1-C	L	NI	T	On	Exp.	0.5, 1,2 BRB	25	1.5 kHz	N/A	99.7
[82] (2019)	1-C, 1-V	L	NI	S	Off*	Exp. &Sim.	1, 2, 4 BRB	0-100	3.84 kHz	U/K	99.34-100
	1-C, 1-V	IN	NI	S	Off*	Exp.	1, 2, 4 BRB	0-100	100 kHz	U/K	98.06-98.76
[53] (2019)	6-F	L	I	S	On	Exp. &Sim.	1, 2, 3 BRB	light- high load*	U/K	N/A	U/K
[83] (2020)	1-C	L	NI	S	Off*	Exp.	1, 3, 5, 7 BRB	0-100	30 kHz	N/A	U/K
[33] (2020)	1-C	IN	NI	S	Off*	Exp.	1, 2, 3, 4 BRB	No-high load*	10 kHz	44.4*	Up to 96.5

*: as inferred by authors.

flux that was calculated using FFT was used to detect BBFs. In [86], the frequency spectrum that was obtained by FFT was processed using the independent component analysis (ICA) to extract FFT-ICA features for fault detection and diagnosis in an inverter-fed motor. A similar approach to detect BBFs in a line-fed motor was introduced in [87], where the ICA was supported by artificial neural networks (ANN). Furthermore, the frequency spectrum obtained by FFT was fed to an intelligent multi-agent system for BBFs detection and diagnosis as presented in [88].

In another attempt to overcome the detection BBF in IMs working at very low slip, such as large machines with a very small rated slip or unloaded IMs in off-line tests, an enhanced discrete Fourier transform (DFT) based on zero-padding of the sampled stator current was used in [89] to minimize original FFT spectral leakage. Moreover, DFT with a sliding window and its related sidelobes leakage phenomenon was utilized to detect and diagnose BBFs in [90]. In [59], the FFT followed by the orthogonal matching pursuit algorithm was applied to analyze the vibration signal for BBF detection. In [91], an efficient index to detect BBF under variable loading and different inertia conditions was proposed through the monitoring of the LSH and RSH phase angle variation. Also, another index was proposed to estimate fault severity.

In [46], [47], and [48], the fast Fourier transform was applied to the stator current in the d-q frame to provide a robust basis to discern broken bar from mechanical oscillations. In [46], the magnitude of some frequency components in the active and reactive current spectrum was utilized as a fault indicator. A more advanced fault indicator based on the variation of the magnitude and phase angle of the active and reactive current spectrum was proposed in [47]. Later in [48], it was proved that the d-component of the current is immune from load oscillations and suggested to use of its spectrum as a fault indicator. However, these methods provided efficient methods to detect BBFs under the presence of load oscillations, the three-phase current measurements were required in [46] and three-phase current and voltage measurements were required in [47]. On the other hand, a method was introduced in [34] to avoid the false alarm of BBF and discriminate the BBF from eccentricity fault and load oscillations. In this method, the frequency spectrum of the stray flux collected using a flux sensor was proposed to overcome this problem. In [49], it was proved that the 5^{th} sideband harmonics of the rotor speed in stray or air gab flux are immune to this problem and some other causes of misdiagnosis. But the rotor speed measurement is still a requirement for these methods.

The frequency analysis of the instantaneous power was used for BBFs detection. The BBF-related frequency components are shifted from $(1 \pm 2ks)f_s$ in the current spectrum to $2ksf_s$ in the instantaneous power spectrum far from the fundamental frequency component. Moreover, the results of this method were confirmed in [92]. In addition, it was proved in [92] that the frequency analysis of the instantaneous active and reactive power and their derived signals—the power factor and its phase angle could provide a robust base for differentiating BBF and eccentricity faults from load oscillations.

2) ENVELOP SPECTRUM ANALYSIS-BASED METHODS

Another solution to discriminate the sideband harmonics from the fundamental current component was proposed in [93], [94], and [95]. This solution was based on applying the Hilbert transform (HT) to the sampled current to calculate the current analytical signal or the current envelope. The spectrum analysis of the analytical signal using FFT showed that the main sideband harmonic transferred to $2sf_s$. Furthermore, ANN was used in [94] and [95] to identify BBFs in inverter-fed motor and line-fed motor respectively. Also, [96] provided a solution for detecting BBF under light loading conditions with a relatively small number of samples. In this method, the analytic current signal (current envelope) obtained by a low-cost time-shift-based method was processed using multicoset sampling method at a very low sampling rate. On the other hand, HT was applied to starting current to get its envelope and the standard deviation of this envelope is utilized for fault detection and diagnosis in [97].

3) HIGH-FREQUENCY RESOLUTION-BASED METHODS

To overcome FFT spectral leakage drawbacks especially at low loading conditions and under mixed faults conditions, high-resolution frequency or frequency estimator techniques are used such as multiple signal classification (MUSIC) in [98] and estimation of signal parameters via rotational invariance techniques (ESPRIT) in [99] but, the high-frequency resolution comes at high computational burden. A proposed solution to decrease the computational burden of MUSIC through the use of frequency estimator and ZOOM technique was introduced in [100]. A model order estimation algorithm to improve frequency estimator efficiency and a fault severity criterion to estimate fault severity were proposed in [101]. The MUSIC technique was modified in [102] to detect incipient BBF in inverter-fed motors through the adjustment of three parameters based on load level and the power source. That is presented as a major limitation of this technique. The selection of the optimum values of these parameters is considered the major limitation of this technique.

4) FUNDAMENTAL FREQUENCY SUPPRESSION-BASED METHODS

In [103], the fundamental frequency component was removed from the current signal using interference suppression techniques. Then the maximum likelihood principle is utilized to estimate the fault-related frequencies followed by the fault severity estimation stage based on a generalized likelihood ratio test. An alternative technique to estimate fault-related components in motor operates at low slip with low acquisition time was presented in [104] based on frequency estimation using two cascaded Taylor-Kalman (TK) filters with a subsampling scheme. Later, an estimation technique called nonlinear least squares was applied to the current signal in [105] to estimate and highly attenuate the fundamental current component by suppressing only the frequency component instead of a frequency band like the previous methods. Hence, a clear spectrum that shows fault-related obliviously could be obtained. Moreover, a more simple technique that was based on spectral subtraction, moving average algorithm, and autocorrelation of the stray flux was introduced in [106].

The computational burden of a frequency-based method mainly depends on acquisition time and sampling frequency. So, the BBFs detection method that utilizes a lower sampling frequency without degrading method efficiency is introduced in [107]. This method showed that a low sampling frequency integrated with a notch filter could be efficiently applied with the discrete-time Fourier transform and autoregressive-based spectrum methods to detect BBFs.

5) EMPIRICAL MODE DECOMPOSITION-BASED METHODS

Empirical mode decomposition (EMD) was used as another tool to decompose the current signal into its intrinsic mode functions (IMFs) in [108]. The standard deviation of the samples and the time between successive zero crossings of two current IMFs were presented in [108] as fault indicators. As the EMD has many limitations such as mode mixing problems, stopping criteria, and border effects, Complete Ensemble Empirical Mode Decomposition (CEEMD), a more advanced version of EMD, was presented in [109] to decompose acoustic sound and vibration signals to its IMFs. Then, the spectrum of some IMFs was estimated using the marginal frequency of the Gabor representation and introduced as a fault indicator.

6) COMPARISON OF FREQUENCY-DOMAIN-BASED METHODS

A detailed comparison among different frequency-domain-based fault detection methods introduced in the literature from the year 2004 to 2022 is presented in Table. 7. The comparison covers the number and type of required sensors, tested state (either steady-state or transient), type of IM supply (either line-fed mode. or inverter-fed mode), the severity of tested BBFs, and loading conditions. It also shows the sampling frequency and training required and finally evaluates the achieved accuracy.

C. TIME-FREQUENCY DOMAIN-BASED METHODS FOR BBF DETECTION AND DIAGNOSIS

The conceptual basis of these methods is to use multiple signal processing techniques which are applied to monitor fault-related conditions in the time-frequency domain. Such techniques were introduced in the literature to identify the fault-related components under the transient conditions in the time-frequency $(t-f)$ plane.

1) LINEAR T-F TRANSFORMS-BASED METHODS

In [110], the fractional Fourier transform was applied to the current signal after being filtered using wavelet transform (WT) to extend the capabilities of Fourier transform to deal with the whole range of the motor speed under transient conditions. Then, linear transforms were widely applied to the current, flux signals to evaluate the main side-band harmonics in the $(t-f)$ plane. Such transformers include short-time Fourier transform (STFT), WT, Stockwell transform (ST), adaptive slope transform (AST), and chirplet Transform (CT). The STFT utilizes a fixed time and frequency resolution window dependent on the Heisenberg uncertainty principle. i.e. the improvement of frequency resolution worsen time resolution and vice versa. The resolution of this window cannot be changed from one point to another which represents the major weakness of this transform. In the literature, the STFT was used to detect BBFs in the $(t-f)$ domain in [111] during start-up and counter-current braking respectively. In [112], STFT supported by Otsu segmentation was utilized to early detect and classify BRB faults in IMs under starting of line-fed IMs is proposed. In addition, the STFT was applied to stray flux to detect BBFs in [24], [28], [55], and [113].

In contrast, the window width in the WT is variable and depends on the frequency of the analyzed signal. Therefore, this window provides a high-frequency resolution with a lower time resolution at low frequencies whereas; a

TABLE 7. Comparison among different frequency-domain-based fault detection methods discussed in Section V-B.

[Reference] (year)	Number-sensor type	L/IN	I/NI	S/T	On/off	Type of validation	Fault severity	Loading (%)	Sampling frequency	Training (%)	Accuracy (%)
[84] (2014)	1-F	L	I	S	On*	Exp. &Sim.	1, 2, 4, 6 BRB	Variable loading*	10 kHz	N/A	U/K
[85] (2021)	1-F	L	I	S	Off*	Exp.	1, 2 BRB	U/K	6 kHz	N/A	U/K
[34] (2020)	1-F	L	NI	S	Off*	Exp. &Sim.	1 BRB	100*	10 kHz	N/A	U/K
[86] (2016)	1-C	IN	NI	S	On	Exp. &Sim.	0.5, 1, 2 BRB	0-100	50 kHz	20	100
[87] (2019)	1-C	L	NI	S	Off*	Exp.	0.5, 1 BRB	50-75	3.2 kHz	70	90-99
[88] (2020)	1-C	L	NI	S	Off*	Exp.	1, 2, 3 BRB	U/K	2 GHz	50-75	81.3–89.4
[89] (2021)	1-C	L	NI	S	Off*	Exp.	U/K	U/K	5 kHz	N/A	U/K
[90] (2017)	1-C	IN	NI	S	On*	Exp.	1 BRB	0-90	3 kHz	N/A	U/K
[59] (2018)	3-VS	L	NI	S	Off*	Exp.	Partial, 1 BRB	0-100	3.2 kHz	58.33	90
[91] (2022)	1-C, 1-V	L	NI	S	Off	Exp.	Partial, 1, 2 BRB	10-100	5, 12 kHz	N/A	100
[92] (2012)	3-C, 3-V	L	NI	S	On*	Exp.	1 BRB	U/K	U/K	N/A	U/K
[107] (2008)	1-C, 1-S	IN	NI	S	On*	Exp.	1 BRB	100	200 Hz	N/A	U/K
[93] (2009)	1-C	L	NI	S	On & Off	Exp.	1 BRB	0-100	10 kHz	N/A	U/K
[94] (2020)	1-C	IN	NI	T	On	Exp. &Sim.	1, 2 BRB	100	U/K	U/K	70.4-99.99
[95] (2016)	1-C	L	NI	S	Off*	Sim.	1, 2 BRB	Low-High load	U/K	U/K	U/K
[96] (2017)	1-C	IN	NI	S	Off*	Exp.	1 BRB	3-100	2 kHz	U/K	U/K
[97] (2017)	1-C	L&IN	NI	T	Off*	Sim.	0.5, 1, 1.5 BRB	0-100	U/K	U/K	U/K
[98] (2012)	1-C	L	NI	S	On*	Exp.	1 BRB	U/K	1.5 kHz	N/A	U/K
[99] (2013)	1-C	L	NI	S	On	Exp.	1 BRB	0	1 kHz	N/A	U/K
[100] (2013)	1-C	IN	NI	S	On	Exp.	1, 2 BRB	0-100%	100-200 kHz	N/A	U/K
[101] (2016)	1-C	IN	NI	S	Off*	Exp.	1, 2, 3 BRB	U/K	20 kHz	N/A	U/K
[102] (2017)	1-C	L&IN	NI	S	Off*	Exp.	Partial, 1, BRB	Medium-High load	50 kHz	N/A	U/K
[103] (2017)	1-C	IN	NI	S	Off	Exp. &Sim.	1, 2 BRB	50	20 kHz	N/A	U/K
[104] (2018)	1-C	L	NI	S	Off*	Exp. &Sim.	U/K	U/K	3.03 & 6.6 kHz	N/A	U/K
[105] (2019)	1-C*	IN	NI	S	Off*	Exp.	1 BRB	20	4 kHz & 8 kHz	N/A	99%
[106] (2019)	1-F	L	NI	S	Off*	Exp.	2 BRB	U/K	5 kHz	N/A	U/K
[108] (2015)	1-C	L	NI	S&T	On	Exp.	Partial, 1BRB	50-75	3.2 kHz	U/K	98.2-99.7
[109] (2017)	3-VS, 1-A	L	NI	S&T	On*	Exp.	2 BRB	100%*	1.5-2 kHz	N/A	U/K
[123] (2017)	3-C	L	NI	S	Off*	Exp. &Sim.	1, 2 BRB	Low-rated load	≥1 kHz	N/A	U/K

*: as inferred by the authors.

low-frequency resolution with a higher time resolution at high frequencies can be obtained. In the literature, the continuous wavelet transform (CWT) was applied to the current signal in the starting to detect BBFs pattern in [114] and [115]. In [116], the STFT, CWT, and a multilabel classification framework were applied to detect BBFs in the starting of a line-fed motor. In addition, the synchro-squeezing transform that is based on CWT but with a higher *t-f* resolution is used to detect the same fault in [117]. The DWT that is discretized form of CWT was utilized in [27] to detect BBFs using the current signal. The energy eigenvalues of these frequency bands under steady-state condition were utilized as a fault indicator in [118] whereas, a fault indicator related to a certain frequency band under transient conditions were proposed in [27]. An outstanding performance method was applied in [119] to detect multiple motor faults online at early stages regardless of motor characteristics. In this method, a wavelet function and a multivariate control chart were applied to the current signal in the steady-state to detect and classify BBFs regardless of the supply mode. In contrast, the energy of sub-bands extracted from the acoustic signals using rational-dilation wavelet transform was presented as a useful fault indicator in [61].

Later, DWT is combined with Local Binary Pattern to extract features from the acoustic signal as presented in [120]. Neighborhood Component Analysis, Support Vector Machine, and K Nearest Neighborhood were utilized to select the most informative features and classify BBFs.

Furthermore, a multiple-windowed harmonic wavelet packet transform (WPT) as a modified version of the DWT was introduced in [121] to overcome the problem of continuous redefinition of the decomposition tree levels to deal

with the variable frequency content in the case of inverter-fed motors. In [11], WPT was applied to the vibration signal to detect BBF. However, WT has many limitations such as dependence on the mother wavelet and number decomposition levels [13].

Also, to automatically detect and diagnose early BBF under the variable loading and inertia conditions without the need for expert knowledge, a method that is based on ST was applied in [13]. The ST that have a variable window width with more control parameters for better resolution adjustment than WT. In such study, the window width control parameters were selected using an active-set optimization technique and the ST was applied to the current signal to detect and diagnose BBFs in a directly fed motor.

As the previous linear transforms, AST is subjected to trade-off between time and frequency resolution. Nevertheless, the AST has a major benefit over STFT and WT in that the window can be adjusted at every point in *t-f* plane. Consequently, the trajectory of the LSH and RSH can be represented efficiently. Actually, the AST was utilized in [25] and [122] to detect BBFs of a line-fed motor and inverter-fed motor respectively.

The chriplet transform (CT) shares the same feature with other linear transformers. On the other hand, CT does not follow the *t-f* trade-off rule like other linear transformers [25]. While the window of STFT for example has a definite length and width in the *t-f* plane, the window of CT provides only thickness and direction [25]. Therefore, the CT represents one of the most suitable linear transforms to monitor LSH and RSH in the case of BBFs in inverter-fed motors. It is worth mentioning that the CT is not suitable for analyzing signals that change their directions in the *t-f* plane abruptly. In [124], the CT was applied to the current signal of an inverter-fed IM operating at low slip conditions where the fault component frequencies are very close to the fundamental component in the *t-f* plane.

Based on the previous discussion, it can be deduced that the CT can efficiently monitor LSH and RSH in the case of the inverter-fed motor during starting whereas, AST can monitor these fault-related harmonics during steady-state. To overcome the shortcoming of AST and CT, the dragon transform (DT) was introduced in [38] and [125]. The DT employs a more advanced window, so it can efficiently represent the trajectories of the fault-related components during starting and steady-state in both line-fed and inverter-fed modes under sophisticated control algorithms.

2) QUADRATIC T-F DISTRIBUTION-BASED METHODS

In the literature, another type of *t-f* representation called quadratic *t-f* distribution is presented. In this type, a higher time and frequency resolution can be provided simultaneously. However, this type suffers from cross terms drawbacks when analyzing multicomponent signals. The Wigner-Ville Distribution (WVD) represents this type of *t-f* distribution. In [126] and [127], the WVD was applied to the starting current of a direct-fed motor and the steady state current of an inverter-fed motor in [128]. Also, another type of quadratic distribution, called Zhao-Atlas-Marks (ZAM) distribution, was applied to vibration signals to detect BBFs in [129]. To limit the cross terms that degrade the quality of WVD, a filtered current signal during starting of a direct-fed motor was used instead of the original signal as in [130].

3) HILBERT-HUANG TRANSFORM-BASED METHODS

Moreover, the Hilbert-Huang Transform (HHT) was introduced in the literature to detect the BBFs in both modes of supply. This transform is based on the decomposition of the analyzed signal to a number of IMFs using EMD to be more suitable to be processed using the HT [25]. The HT can accurately define the instantaneous frequency of each IMF and its amplitude. More advanced decomposition algorithms like the Ensemble Empirical Mode Decomposition (EEMD) and Variational Mode Decomposition (VMD) are introduced in the literature to overcome EMD problems (discussed before in Section V. B-6). The HHT was presented in [131] and [132] to detect BBFs in line-fed and inverter-fed modes under steady-state respectively, while, in [133] and [134], the HHT was applied to detect BBFs in the line-fed mode under transient conditions.

4) HIGH T-F RESOLUTION-BASED METHODS

In another attempt to improve the *t-f* resolution, the high-resolution frequency method such as MUSIC was presented in the literature to detect BBFs, especially in the case of inverter-fed mode. In [135], the current signal was decomposed by CEEMD and the resulting IMFs were processed using MUSIC algorithm to detect BBFs in both steady-state and starting inverter-fed motors. In fact, this method and the method based on DT have an outstanding performance compared to other transforms, especially in inverter-fed mode. Later, a method based on MUSIC and non-uniform demodulation was applied in [136] on the current signal to detect BBFs in the inverter-fed mode under starting conditions. In [137], a non-uniform sampling technique and MUSIC were used to change the trajectories of LSH and RSH in the *t-f* plane in the case of starting an inverter-fed motor to be easily monitored. In addition, the MUSIC algorithm was applied to the zero-sequence current in [6] to detect such faults in line-fed mode.

5) COMPARISON OF T-F DOMAIN-BASED METHODS

A detailed comparison among several reported time-frequency domain-based fault detection methods (28 references published from 2008 to 2021) in the literature is presented in Table. 8.

Also to illustrate the difference in the resolution between some *t-f* transforms, some *t-f* representations are presented in Fig. 10, for the current signal of a real motor with one broken bar has the following characteristics: 400 V, 1.5 kW, 2-poles, 3.25 A, and 2860 rpm at full load.

TABLE 8. Comparison among different time-frequency domain-based fault detection methods discussed in Section V-C.

[Reference] (year)	Number-sensor type	L/IN	I/NI	S/T	Transform	Type of validation	Fault severity	Sampling frequency	*t-f* resolution
[111] (2017)	1-C	L	NI	T	STFT	Exp.	1, 3 BRB	12.8 kHz	++
[112] (2020)	1-C	L	NI	T	STFT	Exp.	0.5, 1, 2 BRB	1.5 kHz	++
[24] (2019)	1-F	L	NI	S & T	STFT	Exp. &Sim	2 BRB	5 kHz	++
[28] (2020)	1-F/1-F	L	I/NI	S & T	STFT	Exp. &Sim	1, 2 BRB	6 kHz	++
[55] (2018)	1-F	L	NI	S & T	STFT	Exp.	2 BRB	5 kHz	++
[113] (2019)	1-F	L	NI	S & T	STFT	Sim.	2 BRB	U/K	++
[114] (2011)	1-C	L	NI	T	CWT	Exp.	1, 2, 3 BRB	U/K	++
[27] (2014)	1-C	L	NI	T	DWT	Exp. &Sim.	1, 2 BRB	10.24 kHz	N/A
[61] (2018)	1-A	L	NI	S	DWT	Exp.	U/K	22.1 kHz	N/A
[118] (2010)	1-C*	L	NI	S	DWT	Exp.	1, 2 BRB	10 kHz	N/A
[119] (2017)	1-C	L&IN	NI	S	DWT	Exp.	Partial, 1, BRB	80 kHz	N/A
[120] (2021)	1-A	L	NI	S	DWT	Exp.	1, 2, 3 BRB	44 kHz	N/A
[121] (2020)	1-C	IN	NI	S&T	WPT	Exp.	1 BRB	700 Hz	N/A
[115] (2013)	1-C	L	NI	T	CCWT	Exp.	1 BRB	1 kHz	++
[116] (2017)	1-C	L	NI	T	STFT+ CWT	Exp.	1 BRB	U/K	N/A
[11] (2021)	1- VS	L	NI	S	WPT	Exp.	1 BRB	10 kHz	N/A
[122] (2016)	1-C	L	NI	T	AST	Exp.	1 BRB	U/K	+++
[13] (2021)	1-C	L	NI	T	ST	Exp. &Sim.	1, 2, 3, 4 BRB	5 kHz	+++
[124] (2014)	1-C	IN	NI	T	CT	Exp.	1 BRB	5 kHz	+++
[38] (2021)	1-C	IN	NI	S & T	DT	Exp.	1 BRB	60 kHz	++++
[125] (2021)	1-C	IN	NI	S & T	DT	Exp.	1 BRB	5 kHz	++++
[129] (2013)	2-VS	L	NI	T	ZAM	Exp.	1 BRB	10 kHz	++
[128] (2015)	1-C	IN	NI	S	WVD	Exp.	1 BRB	5 kHz	++
[127] (2020)	1-C	L	NI	T	WVD	Exp.	1 BRB	5 kHz	++
[132] (2021)	1-C	L	NI	S	HHT	Exp.	2 BRB	1 kHz	N/A
[131] (2014)	1-C	IN	NI	S	HHT	Exp.	1, 3 BRB	25.6 kHz	+++
[133] (2017)	1-C	L	NI	T	HHT	Exp.	Partial, 1 BRB	3.2 kHz	+++
[134] (2019)	1-C	L	NI	T	HHT	Exp.	1 BRB	1 kHz	+++
[135] (2016)	1-C	IN	NI	S & T	CEEMD+MUSIC	Exp.	1 BRB	5 kHz	++++
[136] (2019)	1-C	IN	NI	T	MUSIC	Exp.	1 BRB	12 kHz	++++
[6] (2018)	1-C	L	NI	T	MUSIC	Exp. &Sim.	1,2 BRB	5 kHz	+++
[137] (2017)	1-C, 1-V	IN	NI	T	MUSIC	Exp.	1 BRB	12 kHz	+++

*: as inferred by authors.

D. DISCUSSION ON SIGNAL PROCESSING-BASED METHODS FOR BBF DETECTION AND DIAGNOSIS

As discussed before, the fault-related features are extracted in signal processing-based methods from the time, frequency, and time-frequency domains. Accordingly, some issues are summarized regarding the implementation of these methods as follows:

- Statistical features are generally extracted from the signal in the time domain. Therefore, the computational burden of these features' processing is low compared to other signal processing–based methods. However, an artificial or statistical classifier is required for fault severity diagnosis and hence classifier training is required.
- In contrast, when the fault-related features are extracted from the frequency domain, the diagnosis of BBFs is based on monitoring the magnitude of fault-related frequency components mainly LSH and RSH. These frequencies are strictly close to the fundamental components, especially in case zero and low loading conditions. In addition, in the inverter-fed mode, harmonics of high levels are injected into the current that may flood fault-related frequencies. Therefore, the main contributions in this field can be concluded in:
  - Suppressing fundament components and harmonics for better monitoring of LSH and RSH,
  - Applying high-resolution methods to clearly show fault-related frequencies,
  - Monitoring frequencies in the current envelop or instantaneous power where the frequencies of interest are from fundamental components and monitoring frequency band rather than certain frequencies.
  - Although, the frequency-based methods are the common BBFs detection method, they require more computational burden than time–based methods. In addition, a threshold determination for fault detection or a classifier may be required.
- In the time-frequency domain-based methods, the fault-related features are extracted from the *t-f* plane

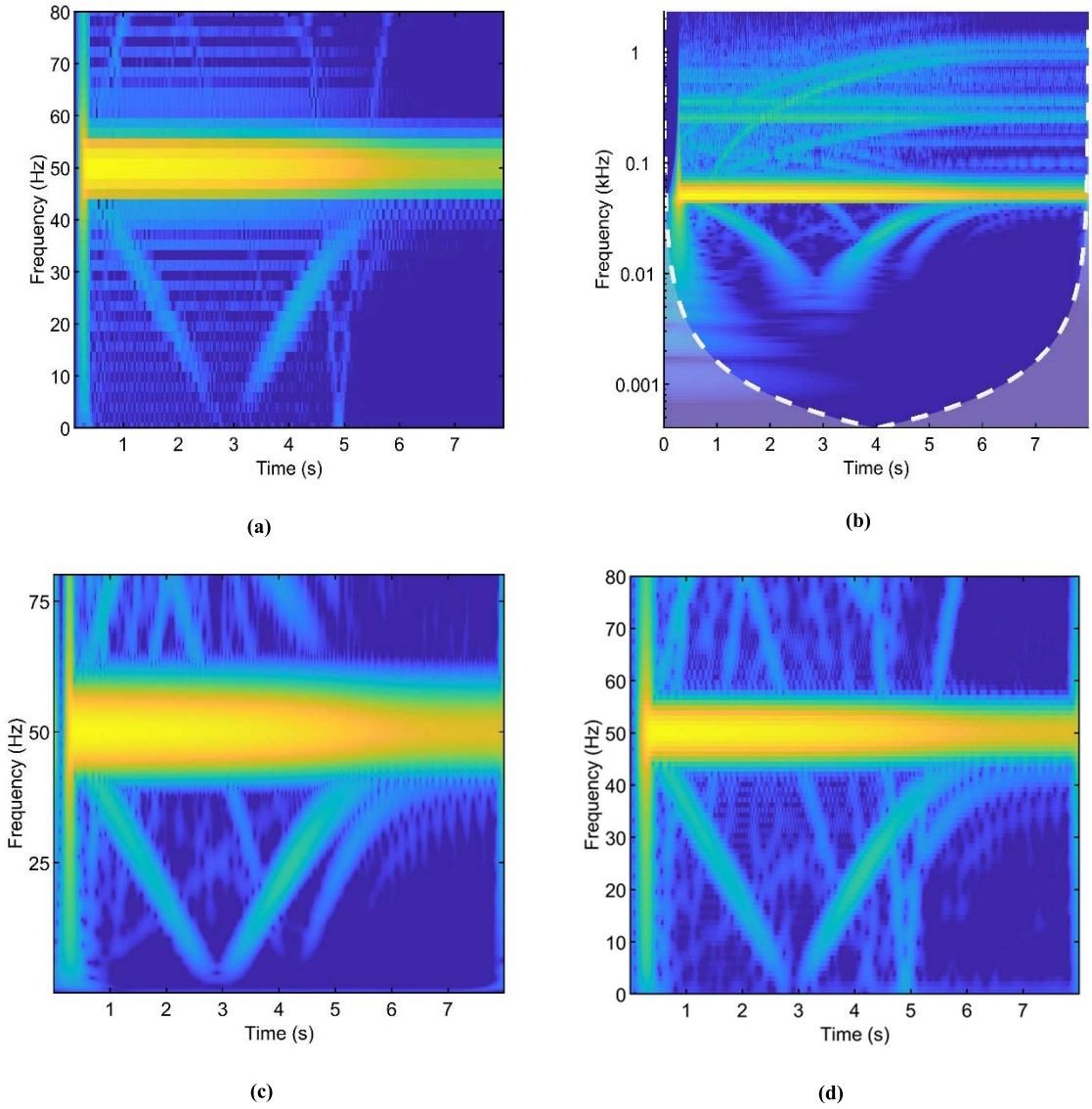

FIGURE 10. Time-Frequency representation of real current signal of induction motor with one broken bar (developed by authors and obtained based on real data) (a) STFT, (b) CWT, (c) Optimized Stockwell transform, and (d) Chirplet Transform (developed by authors and obtained by simulation tests).

generally during starting conditions. The fault-related features appear as a unique pattern in the *t-f* plane in the case of line-fed mode and as two lines strictly close to the fundamental components. Therefore, the detection of BBFs in the case of inverter-fed modes is more challenging. Although the detection of BBFs is easier than the previous two approaches, the transformers used in these methods require more computational burden. In addition, expert knowledge is required for fault identification. The Persistence Spectrum may be a potential solution that we suggest to overcome the challenges associated with detecting fault-related components in inverter-fed modes with a suitable calculation burden [138], [139]. It is widely used to detect the hidden weak signals in other powerful signals.

VI. DATA-DRIVEN-BASED METHODS FOR BBF DETECTION AND DIAGNOSIS

In this approach, the data-driven methods are applied directly to the measured signals to detect and estimate the severity of the fault with high accuracy [140]. These methods, in contrast to the model-based methods and signal-processing-based methods, expert experience to select and extract fault features is not required. On the other hand, the data-driven-based methods do not provide the physical interpretation for fault detection and diagnosis [140]. In addition, a considerable amount of training data is required to achieve reasonable accuracy [22]. In an industrial environment, providing a large amount of data for training may be unavailable and require a high computational burden [22], [141]. The learning strategy of the data-driven methods can be classified as supervised and unsupervised [22]. In the unsupervised learning strategy,

TABLE 9. Comparison among different Data-driven based methods discussed in Section VI.

[Reference] (year)	Number-sensor type	L/IN	I/NI	Method	Type of validation	Fault severity	Sampling frequency	Training (%)	Accuracy (%)
[142] (2016)	1-Vs	IN	NI	DNN	Exp.	3 BRB	20 kHz	66.67	> 96
[143] (2020)	1-C	L	NI	deep-SincNet	Exp.	1, 2 BRB	12 kHz	75	99.9
[144] (2021)	3-Vs	L	NI	ADG-dCNN	Exp.	1, multi-BRB	10 kHz	21.4	99.70
[145] (2021)	4- Vs*	L*	NI	NBC+ IKDE	Exp.	2 BRB	51.2 kHz	70	U/K
[146] (2019)	1-C	IN	NI	Auto-encoder	Exp.	U/K	20 kHz	70	96.1
[147] (2021)	4-A	IN	NI	NDAmSDA	Exp.	U/K	44.1 kHz	U/K	97.1*
[148] (2020)	1-C	L	NI	CNN	Exp.	0.5, 1, 2 BRB	1.5 kHz	75	100
[149] (2021)	1-F	L	NI	CNN	Exp.	1, 2 BRB	5 kHz	80	66.7
[150] (2019)	1-C	L	NI	CNN	Exp.	1, 2 BRB	128 Hz	U/K	97.9

*: as inferred by authors.

the knowledge base is extracted from the historical unlabeled data to simulate healthy system behavior, which is used to judge the real-time system behavior [22]. So, the unsupervised learning strategy depends on the AI to detect hidden patterns in the provided data without human aid. Whereas, in the supervised learning strategy the knowledge bases for both healthy and faulty conditions are extracted from labeled data that are used for system monitoring [22].

In the literature, an unsupervised learning technique was used in [142] to detect and diagnose BBFs where a deep neural network (DNN) was trained using features extracted by sparse auto-encoder from unlabeled data, and a dropout algorithm was utilized to avoid overfitting during the training stages. The deep-SincNet method supported with a convolutional neural network (CNN) represents another example of an unsupervised learning technique implemented in [143] to detect BBFs using the current signal with high accuracy for single and mixed faults in noisy environments. Whereas a supervised learning approach was utilized in [144], where an adaptive gradient optimizer-based deep convolutional neural network (ADG-dCNN) technique was introduced to automatically detect BBFs using multi-vibration sensors with minimum human intervention. Another data-driven approach that was based on Interpolated Kernel Density Estimator (IKDE) was utilized in [145] due to its superiority over other Kernel Density Estimators in terms of speed improvement and computational burden. Where the Naive Bayes Classifier (NBC) supported with Interpolated Kernel Density Estimate (IKDE) was presented to detect and classify BBFs using multi-vibration sensors. Furthermore, auto-encoder networks were used for BBF detection and diagnosis utilizing both labeled and unlabeled data. In [146], stacked auto-encoder networks were used to extract fault features from the current signal in the frequency domain using labeled data. This method could screen false alarms and detect inter-turn, BBFs, and bearing faults while reducing expertise demand. In [147], a Noisy Domain Adaptive marginal Stacking Denoising Auto-encoder (NDAmSDA) technique was employed to detect and classify BBFs based on an acoustic signal using an unsupervised learning approach. On the other hand, a method for early detection and classification of BBFs was proposed in [148] based on using 2-D CNN to classify *t-f* images obtained by applying STFT to starting current after removing the fundamental current component using a notch filter. A relatively similar approach was proposed in [149], but images were obtained by applying STFT to stray flux during starting. In [150], shallow and adaptive 1-D CNN was proposed to automatically extract features from the raw current signal and classify faults with high accuracy.

The main advantages of shallow CNN over deep CNN are suitability for real-time application, limited data required for training, and cost-effective implementation [150]. On the other hand, deep CNN and DNN have more advanced feature extraction and learning abilities [144]. However, DNN suffers from some drawbacks such as overfitting, high computational burden, and the selection of its parameters becomes challenging for complicated problems [144]. In contrast, deep CNN requires less computational burden than DNN as it utilizes fewer connections between layers than DNN resulting in less probability of overfitting [144]. In general, the deep models are more efficient in feature extraction and more suitable for BBF than shallow ones.

A comparison among different data-driven-based fault detection methods introduced in the literature is presented in Table. 9.

However, the data-driven approach can independently extract features from the row signals without the need for signal processing tools. This advantage comes at a high cost of computational burden and the amount of data required for training that may not be available in the industrial environment. Also, the data-driven-based methods do not provide any physical interpretation for fault detection and diagnosis [140]. On the other hand, the classical approach including model-based methods and signal processing–based methods provides a good physical interpretation and requires a relatively low amount of data. But, expert knowledge is required to build detailed models or manually extract fault features. In our point of view, hybrid techniques which are

a combination between data-driven and classical approaches are the most promising techniques for BBF fault detection and diagnosis. As these techniques provide the main advantages of both approaches. Methods in [151], [152], and [153] are examples of this approach.

VII. CONCLUSION AND IDEAS FOR FUTURE WORK

In this paper, a comprehensive review of the most recent BBFs detection and diagnosis methods up-to-date are provided. The BBFs fault signatures on different motor variables are discussed. In addition, the fault detection and diagnosis methods are classified into: groups and sub-groups to be deeply described and evaluated. A comparison between different methods in the same group and sub-group is presented in a tabulated format for easy interpretation. Additionally, a comprehensive discussion of such methods is offered.

Although the development achieved in the field of BBFs detection and diagnosis, some issues that still require more attention from researchers can be summarized and highlighted in:

- A complete and integrated system for different IM faults identification including broken bar, stator inter-turn, bearing, and eccentricity faults is still required.
- However, model-based methods are one of the most promising methods, the investigation of the performance of model-based methods in the case of the presence of false diagnosis sources such as low-frequency load oscillations and with a lesser number of sensors is still needed.
- The digital twin approach represents a trending technology in the field of monitoring and fault detection, however, a comprehensive application that can detect and diagnose different motor faults is still missing.
- Another alternative to fulfill the requirements is the data-driven-based methods but a relatively large amount of data is required. To overcome this drawback, transfer learning may be a promising solution.
- Regarding signal processing-based methods, the development of methods that provide high accuracy and require low sampling frequency, short acquisition time, and a low computational burden is needed.
- In the time-frequency-based methods, a well-experienced operator is required to identify fault patterns from the *t-f* plane. So, a numerical indicator is required for easy fault detection. Also, the performance of these methods under short-start duration is needed to be more investigated.
- On the other hand, the papers that discuss end ring faults detection in the literature are still rare so; more research is required on this point.

REFERENCES

[1] J. Rangel-Magdaleno, J. Ramirez-Cortes, and H. Peregrina-Barreto, "Broken bars detection on induction motor using MCSA and mathematical morphology: An experimental study," in *Proc. IEEE Int. Instrum. Meas. Technol. Conf. (I2MTC)*, Minneapolis, MN, USA, May 2013, pp. 825–829.

[2] P. Zhang, Y. Du, T. G. Habetler, and B. Lu, "A survey of condition monitoring and protection methods for medium-voltage induction motors," *IEEE Trans. Ind. Appl.*, vol. 47, no. 1, pp. 34–46, Jan./Feb. 2011.

[3] H. Li, G. Feng, D. Zhen, F. Gu, and A. D. Ball, "A normalized frequency-domain energy operator for broken rotor bar fault diagnosis," *IEEE Trans. Instrum. Meas.*, vol. 70, pp. 1–10, 2021.

[4] S. Bindu and V. V. Thomas, "Diagnoses of internal faults of three phase squirrel cage induction motor—A review," in *Proc. Int. Conf. Adv. Energy Convers. Technol. (ICAECT)*, Manipal, India, Jan. 2014, pp. 48–54.

[5] S. Sridhar, K. U. Rao, M. S. Nihaal, and A. K. S. Aashik, "Real time wireless condition monitoring of induction motor," in *Proc. IEEE Ind. Electron. Appl. Conf. (IEACon)*, Kota Kinabalu, Malaysia, Nov. 2016, pp. 173–178.

[6] D. Morinigo-Sotelo, R. de J. Romero-Troncoso, P. A. Panagiotou, J. A. Antonino-Daviu, and K. N. Gyftakis, "Reliable detection of rotor bars breakage in induction motors via MUSIC and ZSC," *IEEE Trans. Ind. Appl.*, vol. 54, no. 2, pp. 1224–1234, Mar. 2018.

[7] V. G. J. Faiz and G. Joksimović, "Induction motor faults: Basics, developments and laboratory-scale implementation," in *Energy Engineering, Fault Diagnosis of Induction Motors*. Croydon, U.K.: Inst. Eng. Technol., 2017, pp. 71–167.

[8] G. Madescu, M. Biriescu, L. N. Tutelea, M. Mot, M. Svoboda, and I. Boldea, "Experimental investigation of rotor currents distribution in the healthy and faulty cage of induction motors at standstill," *IEEE Trans. Ind. Electron.*, vol. 64, no. 7, pp. 5305–5313, Jul. 2017.

[9] L. Weili, X. Ying, S. Jiafeng, and L. Yingli, "Finite-element analysis of field distribution and characteristic performance of squirrel-cage induction motor with broken bars," *IEEE Trans. Magn.*, vol. 43, no. 4, pp. 1537–1540, Apr. 2007.

[10] P. A. Panagiotou, I. Arvanitakis, N. Lophitis, J. A. Antonino-Daviu, and K. N. Gyftakis, "A new approach for broken rotor bar detection in induction motors using frequency extraction in stray flux signals," *IEEE Trans. Ind. Appl.*, vol. 55, no. 4, pp. 3501–3511, Aug. 2019.

[11] Z. Hosseinpoor, M. M. Arefi, R. Razavi-Far, N. Mozafari, and S. Hazbavi, "Virtual sensors for fault diagnosis: A case of induction motor broken rotor bar," *IEEE Sensors J.*, vol. 21, no. 4, pp. 5044–5051, Feb. 2021.

[12] V. Ghorbanian and J. Faiz, "A survey on time and frequency characteristics of induction motors with broken rotor bars in line-start and inverter-fed modes," *Mech. Syst. Signal Process.*, vols. 54–55, pp. 427–456, Mar. 2015.

[13] M. E. E.-D. Atta, D. K. Ibrahim, and M. I. Gilany, "Broken bar faults detection under induction motor starting conditions using the optimized stockwell transform and adaptive time–frequency filter," *IEEE Trans. Instrum. Meas.*, vol. 70, pp. 1–10, 2021.

[14] M.-Q. Tran, M.-K. Liu, Q.-V. Tran, and T.-K. Nguyen, "Effective fault diagnosis based on wavelet and convolutional attention neural network for induction motors," *IEEE Trans. Instrum. Meas.*, vol. 71, pp. 1–13, 2022.

[15] G. A. Capolino, J. A. Antonino-Daviu, and M. Riera-Guasp, "Modern diagnostics techniques for electrical machines, power electronics, and drives," *IEEE Trans. Ind. Electron.*, vol. 62, no. 3, pp. 1738–1745, Mar. 2015.

[16] M. Riera-Guasp, J. A. Antonino-Daviu, and G.-A. Capolino, "Advances in electrical machine, power electronic, and drive condition monitoring and fault detection: State of the art," *IEEE Trans. Ind. Electron.*, vol. 62, no. 3, pp. 1746–1759, Mar. 2015.

[17] Y. Liu and A. M. Bazzi, "A review and comparison of fault detection and diagnosis methods for squirrel-cage induction motors: State of the art," *ISA Trans.*, vol. 70, pp. 400–409, Sep. 2017.

[18] O. E. Hassan, M. Amer, A. K. Abdelsalam, and B. W. Williams, "Induction motor broken rotor bar fault detection techniques based on fault signature analysis—A review," *IET Electr. Power Appl.*, vol. 12, no. 7, pp. 895–907, Aug. 2018.

[19] A. Bellini, F. Filippetti, C. Tassoni, and G.-A. Capolino, "Advances in diagnostic techniques for induction machines," *IEEE Trans. Ind. Electron.*, vol. 55, no. 12, pp. 4109–4126, Dec. 2008.

[20] H. Henao, G.-A. Capolino, M. Fernandez-Cabanas, F. Filippetti, C. Bruzzese, E. Strangas, R. Pusca, J. Estima, M. Riera-Guasp, and S. Hedayati-Kia, "Trends in fault diagnosis for electrical machines: A review of diagnostic techniques," *IEEE Ind. Electron. Mag.*, vol. 8, no. 2, pp. 31–42, Jun. 2014.

[21] Z. Gao, C. Cecati, and S. X. Ding, "A survey of fault diagnosis and fault-tolerant techniques—Part I: Fault diagnosis with model-based and signal-based approaches," *IEEE Trans. Ind. Electron.*, vol. 62, no. 6, pp. 3757–3767, Jun. 2015.

[22] Z. Gao, C. Cecati, and S. X. Ding, "A survey of fault diagnosis and fault-tolerant techniques—Part II: Fault diagnosis with knowledge-based and hybrid/active approaches," *IEEE Trans. Ind. Electron.*, vol. 62, no. 6, pp. 3768–3774, Jun. 2015.

[23] M. Nemec, V. Ambrožič, R. Fišer, D. Nedeljković, and K. Drobnič, "Induction motor broken rotor bar detection based on rotor flux angle monitoring," *Energies*, vol. 12, no. 5, p. 794, 2019.

[24] P. A. Panagiotou, I. Arvanitakis, N. Lophitis, J. A. Antonino-Daviu, and K. N. Gyftakis, "On the broken rotor bar diagnosis using time–frequency analysis: 'Is one spectral representation enough for the characterisation of monitored signals?'" *IET Electr. Power Appl.*, vol. 13, no. 7, pp. 932–942, Jul. 2019.

[25] V. Fernandez-Cavero, D. Morinigo-Sotelo, O. Duque-Perez, and J. Pons-Llinares, "A comparison of techniques for fault detection in inverter-fed induction motors in transient regime," *IEEE Access*, vol. 5, pp. 8048–8063, 2017.

[26] C. Yang, T.-J. Kang, S. B. Lee, J.-Y. Yoo, A. Bellini, L. Zarri, and F. Filippetti, "Screening of false induction motor fault alarms produced by axial air ducts based on the space-harmonic-induced current components," *IEEE Trans. Ind. Electron.*, vol. 62, no. 3, pp. 1803–1813, Mar. 2015.

[27] C. Yang, T.-J. Kang, D. Hyun, S. B. Lee, J. A. Antonino-Daviu, and J. Pons-Llinares, "Reliable detection of induction motor rotor faults under the rotor axial air duct influence," *IEEE Trans. Ind. Appl.*, vol. 50, no. 4, pp. 2493–2502, Jul./Aug. 2014.

[28] Y. Park, H. Choi, S. B. Lee, and K. N. Gyftakis, "Search coil-based detection of nonadjacent rotor bar damage in squirrel cage induction motors," *IEEE Trans. Ind. Appl.*, vol. 56, no. 5, pp. 4748–4757, Oct. 2020.

[29] F. Briz, M. W. Degner, A. B. Diez, and J. M. Guerrero, "Online diagnostics in inverter-fed induction machines using high-frequency signal injection," *IEEE Trans. Ind. Appl.*, vol. 40, no. 4, pp. 1153–1161, Jul. 2004.

[30] J. A. Antonino-Daviu, K. N. Gyftakis, R. Garcia-Hernandez, H. Razik, and A. J. Marques Cardoso, "Comparative influence of adjacent and non-adjacent broken rotor bars on the induction motor diagnosis through MCSA and ZSC methods," in *Proc. 1st Annu. Conf. IEEE Ind. Electron. Soc.*, Yokohama, Japan, Nov. 2015, pp. 1680–1685.

[31] M. S. Rafaq, M. Faizan Shaikh, Y. Park, and S. B. Lee, "Reliable airgap search coil based detection of induction motor rotor faults under false negative motor current signature analysis indications," *IEEE Trans. Ind. Informat.*, vol. 18, no. 5, pp. 3276–3285, May 2022.

[32] M. A. Hmida and A. Braham, "An on-line condition monitoring system for incipient fault detection in double-cage induction motor," *IEEE Trans. Instrum. Meas.*, vol. 67, no. 8, pp. 1850–1858, Aug. 2018.

[33] C. G. Dias, L. C. da Silva, and W. A. L. Alves, "A histogram of oriented gradients approach for detecting broken bars in squirrel-cage induction motors," *IEEE Trans. Instrum. Meas.*, vol. 69, no. 9, pp. 6968–6981, Sep. 2020.

[34] K. N. Gyftakis, P. A. Panagiotou, and S. B. Lee, "Generation of mechanical frequency related harmonics in the stray flux spectra of induction motors suffering from rotor electrical faults," *IEEE Trans. Ind. Appl.*, vol. 56, no. 5, pp. 4796–4803, Sep. 2020.

[35] A. Naha, A. K. Samanta, A. Routray, and A. K. Deb, "A method for detecting half-broken rotor bar in lightly loaded induction motors using current," *IEEE Trans. Instrum. Meas.*, vol. 65, no. 7, pp. 1614–1625, Apr. 2016.

[36] W. S. Abu-Elhaija, V. Ghorbanian, J. Faiz, and B. M. Ebrahimi, "Impact of closed-loop control on behavior of inverter-fed induction motors with rotor broken-bars fault," in *Proc. IEEE Int. Conf. Power Electron., Drives Energy Syst. (PEDES)*, Bengaluru, India, Dec. 2012, pp. 1–4.

[37] A. Ceban, R. Pusca, and R. Romary, "Study of rotor faults in induction motors using external magnetic field analysis," *IEEE Trans. Ind. Electron.*, vol. 59, no. 5, pp. 2082–2093, May 2012.

[38] V. Fernandez-Cavero, J. Pons-Llinares, O. Duque-Perez, and D. Morinigo-Sotelo, "Detection of broken rotor bars in nonlinear startups of inverter-fed induction motors," *IEEE Trans. Ind. Appl.*, vol. 57, no. 3, pp. 2559–2568, May 2021.

[39] C. Concari, G. Franceschini, C. Tassoni, and A. Toscani, "Validation of a faulted rotor induction machine model with an insightful geometrical interpretation of physical quantities," *IEEE Trans. Ind. Electron.*, vol. 60, no. 9, pp. 4074–4083, Sep. 2013.

[40] J. Faiz, V. Ghorbanian, and B. M. Ebrahimi, "Locating broken bars in line-start and inverter-fed induction motors using modified winding function method," *Electromagnetics*, vol. 32, no. 3, pp. 173–192, Mar. 2012.

[41] J. F. V. G. G. Joksimovic, "Diagnosis of broken bars fault in induction motors," in *Energy Engineering, Fault Diagnosis of Induction Motors*. Croydon, U.K.: Inst. Eng. Technol., 2017, pp. 367–429.

[42] M. Wolkiewicz, G. Tarchala, and T. Orlowska-Kowalska, "Diagnosis of stator and rotor faults of an induction motor in closed-loop control structure," in *Proc. Int. Symp. Power Electron., Electr. Drives, Autom. Motion (SPEEDAM)*, Amalfi, Italy, Jun. 2018, pp. 196–201.

[43] A. Sapena-Bano, J. Burriel-Valencia, M. Pineda-Sanchez, R. Puche-Panadero, and M. Riera-Guasp, "The harmonic order tracking analysis method for the fault diagnosis in induction motors under time-varying conditions," *IEEE Trans. Energy Convers.*, vol. 32, no. 1, pp. 244–256, Mar. 2017.

[44] M. Ouadah, O. Touhami, and R. Ibtiouen, "Novel method for rotor bar fault diagnosis of induction machines containing space harmonics," in *Proc. 8th Int. Conf. Syst. Control (ICSC)*, Marrakesh, Morocco, Oct. 2019, pp. 112–116.

[45] G. R. Bossio, C. H. De Angelo, C. M. Pezzani, J. M. Bossio, and G. O. Garcia, "Evaluation of harmonic current sidebands for broken bar diagnosis in induction motors," in *Proc. IEEE Int. Symp. Diag. Electr. Mach., Power Electron. Drives*, Cargese, France, Aug. 2009, pp. 1–6.

[46] G. R. Bossio, C. H. D. Angelo, J. M. Bossio, C. M. Pezzani, and G. O. Garcia, "Separating broken rotor bars and load oscillations on IM fault diagnosis through the instantaneous active and reactive currents," *IEEE Trans. Ind. Electron.*, vol. 56, no. 11, pp. 4571–4580, Nov. 2009.

[47] S. M. A. Cruz, "An active–reactive power method for the diagnosis of rotor faults in three-phase induction motors operating under time-varying load conditions," *IEEE Trans. Energy Convers.*, vol. 27, no. 1, pp. 71–84, Mar. 2012.

[48] M. Meira, C. Ruschetti, C. Verucchi, G. Bossio, and J. Bossio, "Diagnosis of induction motor faults using the full spectrum of direct and quadrature currents," in *Proc. 19th Workshop Inf. Process. Control (RPIC)*, SAN JUAN, Argentina, Nov. 2021, pp. 1–6.

[49] S. B. Lee, J. Shin, Y. Park, H. Kim, and J. Kim, "Reliable flux based detection of rotor cage faults in induction motors," in *Proc. IEEE 13th Int. Symp. Diag. Electr. Mach., Power Electron. Drives (SDEMPED)*, vol. 1. Dallas, TX, USA, Aug. 2021, pp. 160–166.

[50] M. E. K. Oumaamar, A. Khezzar, M. Boucherma, H. Razik, R. N. Andriamalala, and L. Baghli, "Neutral voltage analysis for broken rotor bars detection in induction motors using Hilbert transform phase," in *Proc. IEEE Ind. Appl. Annu. Meeting*, New Orleans, LA, USA, Sep. 2007, pp. 1940–1947.

[51] G. Petrovic, M. Jadric, and M. Despalatovic, "Detection of broken rotor bar in squirrel-cage induction machines using stator zero-components," in *Proc. 19th Int. Conf. Electr. Mach. (ICEM)*, Rome, Italy, Sep. 2010, pp. 1–6.

[52] Z. Hou, J. Huang, H. Liu, M. Ye, Z. Liu, and J. Yang, "Diagnosis of broken rotor bar fault in open- and closed-loop controlled wye-connected induction motors using zero-sequence voltage," *IET Electr. Power Appl.*, vol. 11, no. 7, pp. 1214–1223, Aug. 2017.

[53] Y. Soleimani, S. M. A. Cruz, and F. Haghjoo, "Broken rotor bar detection in induction motors based on air-gap rotational magnetic field measurement," *IEEE Trans. Instrum. Meas.*, vol. 68, no. 8, pp. 2916–2925, Aug. 2019.

[54] K. Saad and G. Mirzaeva, "Advanced diagnosis of rotor faults in large induction motors based on internal flux measurement," in *Proc. IEEE Ind. Appl. Soc. Annu. Meeting*, Portland, OR, USA, Oct. 2016, pp. 1–8.

[55] J. A. Ramirez-Nunez, J. A. Antonino-Daviu, V. Climente-Alarcon, A. Quijano-Lopez, H. Razik, R. A. Osornio-Rios, and R. D. J. Romero-Troncoso, "Evaluation of the detectability of electromechanical faults in induction motors via transient analysis of the stray flux," *IEEE Trans. Ind. Appl.*, vol. 54, no. 5, pp. 4324–4332, Sep. 2018.

[56] T. Goktas, M. Arkan, M. S. Mamis, and B. Akin, "Broken rotor bar fault monitoring based on fluxgate sensor measurement of leakage flux," in *Proc. IEEE Int. Electr. Mach. Drives Conf. (IEMDC)*, Miami, FL, USA, May 2017, pp. 1–6.

[57] D. De Palo, D. Morinigo-Sotelo, and L. Frosini, "Detectability study of broken rotor bars in induction motors at different loads and supplies," in *Proc. IEEE 12th Int. Symp. Diag. Electr. Mach., Power Electron. Drives (SDEMPED)*, Toulouse, France, Aug. 2019, pp. 101–107.

[58] W. Li and C. K. Mechefske, "Detection of induction motor faults: A comparison of stator current, vibration and acoustic methods," *J. Vib. Control*, vol. 12, no. 2, pp. 165–188, 2006.

[59] C. Morales-Perez, J. Rangel-Magdaleno, H. Peregrina-Barreto, J. P. Amezquita-Sanchez, and M. Valtierra-Rodriguez, "Incipient broken rotor bar detection in induction motors using vibration signals and the orthogonal matching pursuit algorithm," *IEEE Trans. Instrum. Meas.*, vol. 67, no. 99, pp. 2058–2068, Sep. 2018.

[60] Y. Gritli, A. O. Di Tommaso, R. Miceli, F. Filippetti, and C. Rossi, "Vibration signature analysis for rotor broken bar diagnosis in double cage induction motor drives," in *Proc. 4th Int. Conf. Power Eng., Energy Electr. Drives*, Istanbul, Turkey, May 2013, pp. 1814–1820.

[61] S. Hemamalini, "Rational-dilation wavelet transform based torque estimation from acoustic signals for fault diagnosis in a three-phase induction motor," *IEEE Trans. Ind. Informat.*, vol. 15, no. 6, pp. 3492–3501, Jun. 2019.

[62] R. Shahnazi, Q. Zhao, A. H. A. Sari, and T. Jeinsch, "Dynamic nonlinear unknown input observer for fault detection of induction motors," in *Proc. 23rd Iranian Conf. Electr. Eng.*, Tehran, Iran, May 2015, pp. 823–828.

[63] J. W. O'Connell, D. H. Green, B. T. Mills, A. Moeller, S. Kidwell, K. Lee, L. Huchel, and S. B. Leeb, "Nonintrusive ventilation system diagnostics," *IEEE Sensors J.*, vol. 21, no. 17, pp. 19268–19278, Sep. 2021.

[64] G.-A. Capolino, R. Romary, H. Henao, and R. Pusca, "State of the art on stray flux analysis in faulted electrical machines," in *Proc. IEEE Workshop Electr. Mach. Design, Control Diagnosis (WEMDCD)*, vol. 1. Athens, Greece, Apr. 2019, pp. 181–187.

[65] Z. Kanovic, D. Matic, Z. Jelicic, M. Rapaic, B. Jakovljevic, and M. Kapetina, "Induction motor broken rotor bar detection using vibration analysis—A case study," in *Proc. 9th IEEE Int. Symp. Diag. Electr. Mach., Power Electron. Drives (SDEMPED)*, Aug. 2013, pp. 64–68.

[66] T. Ameid, A. Menacer, H. Talhaoui, and I. Harzelli, "Rotor resistance estimation using extended Kalman filter and spectral analysis for rotor bar fault diagnosis of sensorless vector control induction motor," *Measurement*, vol. 111, pp. 243–259, Dec. 2017.

[67] J. Zarei, E. Kowsari, and R. Razavi-Far, "Induction motors fault detection using square-root transformed cubature quadrature Kalman filter," *IEEE Trans. Energy Convers.*, vol. 34, no. 2, pp. 870–877, Jun. 2019.

[68] F. Karami, J. Poshtan, and M. Poshtan, "Detection of broken rotor bars in induction motors using nonlinear Kalman filters," *ISA Trans.*, vol. 49, no. 2, pp. 189–195, Apr. 2010.

[69] S. Bachir, S. Tnani, J. C. Trigeassou, and G. Champenois, "Diagnosis by parameter estimation of stator and rotor faults occurring in induction machines," *IEEE Trans. Ind. Electron.*, vol. 53, no. 3, pp. 963–973, Jun. 2006.

[70] M. Sabouri, M. Ojaghi, J. Faiz, and A. J. M. Cardoso, "Model-based unified technique for identifying severities of stator inter-turn and rotor broken bar faults in SCIMs," *IET Electr. Power Appl.*, vol. 14, no. 2, pp. 204–211, Feb. 2020.

[71] A. Rassolkin, V. Rjabtsikov, V. Kuts, T. Vaimann, A. Kallaste, B. Asad, and A. Partyshev, "Interface development for digital twin of an electric motor based on empirical performance model," *IEEE Access*, vol. 10, pp. 15635–15643, 2022.

[72] V. Rjabtsikov, A. Rassolkin, B. Asad, T. Vaimann, A. Kallaste, V. Kuts, S. Jegorov, M. Stepien, and M. Krawczyk, "Digital twin service unit for AC motor stator inter-turn short circuit fault detection," in *Proc. 28th Int. Workshop Electr. Drives, Improving Rel. Electr. Drives (IWED)*, Moscow, Russia, Jan. 2021, pp. 1–5.

[73] A. Rassolkin, V. Rjabtsikov, T. Vaimann, A. Kallaste, V. Kuts, and A. Partyshev, "Digital twin of an electrical motor based on empirical performance model," in *Proc. 9th Int. Conf. Electr. Power Drive Syst. (ICEPDS)*, St. Petersburg, Russia, Oct. 2020, pp. 1–4.

[74] T. D. Lopes, A. Raizer, and W. V. Júnior, "The use of digital twins in finite element for the study of induction motors faults," *Sensors*, vol. 21, no. 23, p. 7833, Nov. 2021.

[75] J. R. Rivera-Guillen, J. J. de Santiago-Perez, J. P. Amezquita-Sanchez, M. Valtierra-Rodriguez, G. I. Perez-Soto, and M. Trejo-Hernandez, "Time-domain diagnosing algorithm for automatic broken rotor bar detection in induction motors," in *Proc. IEEE Int. Autumn Meeting Power, Electron. Comput. (ROPEC)*, Ixtapa, Mexico, Nov. 2018, pp. 1–5.

[76] C. G. Dias and F. H. Pereira, "Broken rotor bars detection in induction motors running at very low slip using a Hall effect sensor," *IEEE Sensors J.*, vol. 18, no. 11, pp. 4602–4613, Jun. 2018.

[77] S. Tierrafria-Baez, P. M. Calderon-Lopez, V. Cano-Valdez, B. K. Aviles-Diaz, C. Rodriguez-Donate, and E. Cabal-Yepez, "Broken rotor bar detection in induction motors through information entropy analysis on the start-up transient and steady-state current signals," in *Proc. 47th Annu. Conf. IEEE Ind. Electron. Soc.*, Toronto, ON, Canada, Oct. 2021, pp. 1–6.

[78] P. Gangsar and R. Tiwari, "Comparative investigation of vibration and current monitoring for prediction of mechanical and electrical faults in induction motor based on multiclass-support vector machine algorithms," *Mech. Syst. Signal Process.*, vol. 94, pp. 464–481, Sep. 2017.

[79] A. Elez, S. Car, S. Tvoric, and B. Vaseghi, "Rotor cage and winding fault detection based on machine differential magnetic field measurement (DMFM)," *IEEE Trans. Ind. Appl.*, vol. 53, no. 3, pp. 3156–3163, May 2017.

[80] G. Mirzaeva and K. I. Saad, "Advanced diagnosis of rotor faults and eccentricity in induction motors based on internal flux measurement," *IEEE Trans. Ind. Appl.*, vol. 54, no. 3, pp. 2981–2991, May/Jun. 2018.

[81] R. A. Lizarraga-Morales, C. Rodriguez-Donate, E. Cabal-Yepez, M. Lopez-Ramirez, L. M. Ledesma-Carrillo, and E. R. Ferrucho-Alvarez, "Novel FPGA-based methodology for early broken rotor bar detection and classification through homogeneity estimation," *IEEE Trans. Instrum. Meas.*, vol. 66, no. 7, pp. 1760–1769, Jul. 2017.

[82] L. H. B. Liboni, R. A. Flauzino, I. N. da Silva, and E. C. M. Costa, "Efficient feature extraction technique for diagnosing broken bars in three-phase induction machines," *Measurement*, vol. 134, pp. 825–834, Feb. 2019.

[83] D. B. B. de Deus, C. A. N. Sobrinho, F. A. Belo, A. V. Brito, J. G. G. de Souza Ramos, and A. C. Lima-Filho, "Density of maxima approach for broken bar fault diagnosis in low slip and variable load conditions of induction motors," *IEEE Trans. Instrum. Meas.*, vol. 69, no. 12, pp. 9797–9804, Dec. 2020.

[84] C. G. Dias and I. E. Chabu, "Spectral analysis using a Hall effect sensor for diagnosing broken bars in large induction motors," *IEEE Trans. Instrum. Meas.*, vol. 63, no. 12, pp. 2890–2902, Dec. 2014.

[85] J. Shin, Y. Park, and S. B. Lee, "Flux-based detection and classification of induction motor eccentricity, rotor cage, and load defects," *IEEE Trans. Ind. Appl.*, vol. 57, no. 3, pp. 2471–2480, May 2021.

[86] T. Yang, H. Pen, Z. Wang, and C. S. Chang, "Feature knowledge based fault detection of induction motors through the analysis of stator current data," *IEEE Trans. Instrum. Meas.*, vol. 65, no. 3, pp. 549–558, Mar. 2016.

[87] J. E. Garcia-Bracamonte, J. M. Ramirez-Cortes, J. de Jesus Rangel-Magdaleno, P. Gomez-Gil, H. Peregrina-Barreto, and V. Alarcon-Aquino, "An approach on MCSA-based fault detection using independent component analysis and neural networks," *IEEE Trans. Instrum. Meas.*, vol. 68, no. 5, pp. 1353–1361, May 2019.

[88] M. Drakaki, Y. L. Karnavas, A. D. Karlis, I. D. Chasiotis, and P. Tzionas, "Study on fault diagnosis of broken rotor bars in squirrel cage induction motors: A multi-agent system approach using intelligent classifiers," *IET Electr. Power Appl.*, vol. 14, no. 2, pp. 245–255, Feb. 2020.

[89] R. Puche-Panadero, J. Martinez-Roman, A. Sapena-Bano, J. Burriel-Valencia, M. Pineda-Sanchez, J. Perez-Cruz, and M. Riera-Guasp, "New method for spectral leakage reduction in the FFT of stator currents: Application to the diagnosis of bar breakages in cage motors working at very low slip," *IEEE Trans. Instrum. Meas.*, vol. 70, pp. 1–11, 2021.

[90] M. A. Moussa, M. Boucherma, and A. Khezzar, "A detection method for induction motor bar fault using sidelobes leakage phenomenon of the sliding discrete Fourier transform," *IEEE Trans. Power Electron.*, vol. 32, no. 7, pp. 5560–5572, Jul. 2017.

[91] M. E. E.-D. Atta, D. K. Ibrahim, M. Gilany, and A. F. Zobaa, "Adaptive scheme for detecting induction motor incipient broken bar faults at various load and inertia conditions," *Sensors*, vol. 22, no. 1, p. 365, Jan. 2022.

[92] M. Drif and A. J. M. Cardoso, "Discriminating the simultaneous occurrence of three-phase induction motor rotor faults and mechanical load oscillations by the instantaneous active and reactive power media signature analyses," *IEEE Trans. Ind. Electron.*, vol. 59, no. 3, pp. 1630–1639, Mar. 2012.

[93] R. Puche-Panadero, M. Pineda-Sanchez, M. Riera-Guasp, J. Roger-Folch, E. Hurtado-Perez, and J. Perez-Cruz, "Improved resolution of the MCSA method via Hilbert transform, enabling the diagnosis of rotor asymmetries at very low slip," *IEEE Trans. Energy Convers.*, vol. 24, no. 1, pp. 52–59, Mar. 2009.

[94] S. K. Ramu, G. C. R. Irudayaraj, S. Subramani, and U. Subramaniam, "Broken rotor bar fault detection using Hilbert transform and neural networks applied to direct torque control of induction motor drive," *IET Power Electron.*, vol. 13, no. 15, pp. 3328–3338, Nov. 2020.

[95] B. Bessam, A. Menacer, M. Boumehraz, and H. Cherif, "Detection of broken rotor bar faults in induction motor at low load using neural network," *ISA Trans.*, vol. 64, pp. 241–246, Sep. 2016.

[96] A. Naha, A. K. Samanta, A. Routray, and A. K. Deb, "Low complexity motor current signature analysis using sub-Nyquist strategy with reduced data length," *IEEE Trans. Instrum. Meas.*, vol. 66, no. 12, pp. 3249–3259, Dec. 2017.

[97] M. Abd-el-Malek, A. K. Abdelsalam, and O. E. Hassan, "Induction motor broken rotor bar fault location detection through envelope analysis of start-up current using Hilbert transform," *Mech. Syst. Signal Process.*, vol. 93, pp. 332–350, Sep. 2017.

[98] A. Garcia-Perez, R. de Jesus Romero-Troncoso, E. Cabal-Yepez, and R. A. Osornio-Rios, "The application of high-resolution spectral analysis for identifying multiple combined faults in induction motors," *IEEE Trans. Ind. Electron.*, vol. 58, no. 5, pp. 2002–2010, May 2011.

[99] B. Xu, L. Sun, L. Xu, and G. Xu, "Improvement of the Hilbert method via ESPRIT for detecting rotor fault in induction motors at low slip," *IEEE Trans. Energy Convers.*, vol. 28, no. 1, pp. 225–233, Mar. 2013.

[100] Y.-H. Kim, Y.-W. Youn, D.-H. Hwang, J.-H. Sun, and D.-S. Kang, "High-resolution parameter estimation method to identify broken rotor bar faults in induction motors," *IEEE Trans. Ind. Electron.*, vol. 60, no. 9, pp. 4103–4117, Sep. 2013.

[101] Y. Trachi, E. Elbouchikhi, V. Choqueuse, and M. E. H. Benbouzid, "Induction machines fault detection based on subspace spectral estimation," *IEEE Trans. Ind. Electron.*, vol. 63, no. 9, pp. 5641–5651, Sep. 2016.

[102] I. Martin-Diaz, D. Morinigo-Sotelo, O. Duque-Perez, P. A. Arredondo-Delgado, D. Camarena-Martinez, and R. J. Romero-Troncoso, "Analysis of various inverters feeding induction motors with incipient rotor fault using high-resolution spectral analysis," *Electr. Power Syst. Res.*, vol. 152, pp. 18–26, Nov. 2017.

[103] E. Elbouchikhi, V. Choqueuse, F. Auger, and M. E. H. Benbouzid, "Motor current signal analysis based on a matched subspace detector," *IEEE Trans. Instrum. Meas.*, vol. 66, no. 12, pp. 3260–3270, Dec. 2017.

[104] L. A. Trujillo-Guajardo, J. Rodriguez-Maldonado, M. A. Moonem, and M. A. Platas-Garza, "A multiresolution Taylor–Kalman approach for broken rotor bar detection in cage induction motors," *IEEE Trans. Instrum. Meas.*, vol. 67, no. 6, pp. 1317–1328, Jun. 2018.

[105] D. A. Elvira-Ortiz, D. Morinigo-Sotelo, L. Morales-Velazquez, R. A. Osornio-Rios, and R. J. Romero-Troncoso, "Non-linear least squares methodology for suppressing the fundamental frequency in the analysis of electric signals," *Electr. Power Syst. Res.*, vol. 175, Oct. 2019, Art. no. 105924.

[106] M. E. Iglesias-Martinez, P. F. de Cordoba, J. A. Antonino-Daviu, and J. A. Conejero, "Detection of nonadjacent rotor faults in induction motors via spectral subtraction and autocorrelation of stray flux signals," *IEEE Trans. Ind. Appl.*, vol. 55, no. 5, pp. 4585–4594, Sep. 2019.

[107] B. Ayhan, H. J. Trussell, M.-Y. Chow, and M.-H. Song, "On the use of a lower sampling rate for broken rotor bar detection with DTFT and AR-based spectrum methods," *IEEE Trans. Ind. Electron.*, vol. 55, no. 3, pp. 1421–1434, Mar. 2008.

[108] R. Valles-Novo, J. J. Rangel-Magdaleno, J. M. Ramirez-Cortes, H. Peregrina-Barreto, and R. Morales-Caporal, "Empirical mode decomposition analysis for broken-bar detection on squirrel cage induction motors," *IEEE Trans. Instrum. Meas.*, vol. 64, no. 5, pp. 1118–1128, May 2015.

[109] P. A. Delgado-Arredondo, D. Morinigo-Sotelo, R. A. Osornio-Rios, J. G. Avina-Cervantes, H. Rostro-Gonzalez, and R. de Jesus Romero-Troncoso, "Methodology for fault detection in induction motors via sound and vibration signals," *Mech. Syst. Signal Process.*, vol. 83, pp. 568–589, Jan. 2017.

[110] M. Pineda-Sanchez, M. Riera-Guasp, J. A. Antonino-Daviu, J. Roger-Folch, J. Perez-Cruz, and R. Puche-Panadero, "Diagnosis of induction motor faults in the fractional Fourier domain," *IEEE Trans. Instrum. Meas.*, vol. 59, no. 8, pp. 2065–2075, Aug. 2010.

[111] D. G. Jerkan, D. D. Reljić, and D. P. Marčetić, "Broken rotor bar fault detection of IM based on the counter-current braking method," *IEEE Trans. Energy Convers.*, vol. 32, no. 4, pp. 1356–1366, Dec. 2017.

[112] M. Lopez-Ramirez, L. M. Ledesma-Carrillo, F. M. Garcia-Guevara, J. Munoz-Minjares, E. Cabal-Yepez, and F. J. Villalobos-Pina, "Automatic early broken-rotor-bar detection and classification using Otsu segmentation," *IEEE Access*, vol. 8, pp. 112624–112632, 2020.

[113] P. A. Panagiotou, I. Arvanitakis, N. Lophitis, J. A. Antonino-Daviu, and K. N. Gyftakis, "FEM approach for diagnosis of induction machines' non-adjacent broken rotor bars by short-time Fourier transform spectrogram," *J. Eng.*, vol. 2019, no. 17, pp. 4566–4570, Jun. 2019.

[114] J. Pons-Llinares, J. A. Antonino-Daviu, M. Riera-Guasp, M. Pineda-Sanchez, and V. Climente-Alarcon, "Induction motor diagnosis based on a transient current analytic wavelet transform via frequency B-splines," *IEEE Trans. Ind. Electron.*, vol. 58, no. 5, pp. 1530–1544, May 2011.

[115] M. Pineda-Sanchez, M. Riera-Guasp, J. Perez-Cruz, and R. Puche-Panadero, "Transient motor current signature analysis via modulus of the continuous complex wavelet: A pattern approach," *Energy Convers. Manage.*, vol. 73, pp. 26–36, Sep. 2013.

[116] G. Georgoulas, V. Climente-Alarcon, J. A. Antonino-Daviu, I. P. Tsoumas, C. D. Stylios, A. Arkkio, and G. Nikolakopoulos, "The use of a multilabel classification framework for the detection of broken bars and mixed eccentricity faults based on the start-up transient," *IEEE Trans. Ind. Informat.*, vol. 13, no. 2, pp. 625–634, Apr. 2017.

[117] D. Camarena-Martinez, C. A. Perez-Ramirez, M. Valtierra-Rodriguez, J. P. Amezquita-Sanchez, and R. de Jesus Romero-Troncoso, "Synchrosqueezing transform-based methodology for broken rotor bars detection in induction motors," *Measurement*, vol. 90, pp. 519–525, Aug. 2016.

[118] A. Bouzida, O. Touhami, R. Ibtiouen, A. Belouchrani, M. Fadel, and A. Rezzoug, "Fault diagnosis in industrial induction machines through discrete wavelet transform," *IEEE Trans. Ind. Electron.*, vol. 58, no. 9, pp. 4385–4395, Sep. 2011.

[119] L. A. García-Escudero, O. Duque-Perez, M. Fernandez-Temprano, and D. Morinigo-Sotelo, "Robust detection of incipient faults in VSI-fed induction motors using quality control charts," *IEEE Trans. Ind. Appl.*, vol. 53, no. 3, pp. 3076–3085, May/Jun. 2017.

[120] O. Yaman, "An automated faults classification method based on binary pattern and neighborhood component analysis using induction motor," *Measurement*, vol. 168, Jan. 2021, Art. no. 108323.

[121] M. Ali Hmida and A. Braham, "Fault detection of VFD-fed induction motor under transient conditions using harmonic wavelet transform," *IEEE Trans. Instrum. Meas.*, vol. 69, no. 10, pp. 8207–8215, Oct. 2020.

[122] J. Pons-Llinares, M. Riera-Guasp, J. A. Antonino-Daviu, and T. G. Habetler, "Pursuing optimal electric machines transient diagnosis: The adaptive slope transform," *Mech. Syst. Signal Process.*, vol. 80, pp. 553–569, Dec. 2016.

[123] K. N. Gyftakis, A. J. M. Cardoso, and J. A. Antonino-Daviu, "Introducing the filtered park's and filtered extended park's vector approach to detect broken rotor bars in induction motors independently from the rotor slots number," *Mech. Syst. Signal Process.*, vol. 93, pp. 30–50, Sep. 2017.

[124] J. Pons-Llinares, D. Morinigo-Sotelo, O. Duque-Perez, J. Antonino-Daviu, and M. Perez-Alonso, "Transient detection of close components through the Chirplet transform: Rotor faults in inverter-fed induction motors," in *Proc. 40th Annu. Conf. IEEE Ind. Electron. Soc.*, Dallas, TX, USA, Oct. 2014, pp. 3386–3392.

[125] V. Fernandez-Cavero, J. Pons-Llinares, O. Duque-Perez, and D. Morinigo-Sotelo, "Detection and quantification of bar breakage harmonics evolutions in inverter-fed motors through the dragon transform," *ISA Trans.*, vol. 109, pp. 352–367, Mar. 2021.

[126] G. Georgoulas, V. Climente-Alarcon, L. Dritsas, J. A. Antonino-Daviu, and G. Nikolakopoulos, "Start-up analysis methods for the diagnosis of rotor asymmetries in induction motors-seeing is believing," in *Proc. 24th Medit. Conf. Control Autom. (MED)*, Athens, Greece, Jun. 2016, pp. 372–377.

[127] R. Puche-Panadero, J. Martinez-Roman, A. Sapena-Bano, J. Burriel-Valencia, and M. Riera-Guasp, "Fault diagnosis in the slip–frequency plane of induction machines working in time-varying conditions," *Sensors*, vol. 20, no. 12, p. 3398, Jun. 2020.

[128] V. Climente-Alarcon, J. A. Antonino-Daviu, A. Haavisto, and A. Arkkio, "Diagnosis of induction motors under varying speed operation by principal slot harmonic tracking," *IEEE Trans. Ind. Appl.*, vol. 51, no. 5, pp. 3591–3599, Sep./Oct. 2015.

[129] V. Climente-Alarcon, J. A. Antonino-Daviu, F. Vedreno-Santos, and R. Puche-Panadero, "Vibration transient detection of broken rotor bars by PSH sidebands," *IEEE Trans. Ind. Appl.*, vol. 49, no. 6, pp. 2576–2582, Nov./Dec. 2013.

[130] V. Climente-Alarcon, J. A. Antonino-Daviu, M. Riera-Guasp, and M. Vlcek, "Induction motor diagnosis by advanced notch FIR filters and the Wigner–Ville distribution," *IEEE Trans. Ind. Electron.*, vol. 61, no. 8, pp. 4217–4227, Aug. 2014.

[131] J. Faiz, V. Ghorbanian, and B. M. Ebrahimi, "EMD-based analysis of industrial induction motors with broken rotor bars for identification of operating point at different supply modes," *IEEE Trans. Ind. Informat.*, vol. 10, no. 2, pp. 957–966, May 2014.

[132] C.-Y. Lee and W.-C. Lin, "Induction motor fault classification based on ROC curve and t-SNE," *IEEE Access*, vol. 9, pp. 56330–56343, 2021.

[133] J. Rangel-Magdaleno, H. Peregrina-Barreto, J. Ramirez-Cortes, and I. Cruz-Vega, "Hilbert spectrum analysis of induction motors for the detection of incipient broken rotor bars," *Measurement*, vol. 109, pp. 247–255, Oct. 2017.

[134] B. D. E. Cherif, A. Bendiabdellah, and S. Seninete, "A comparative study between two stator current HHT and FFT techniques for IM broken bar fault diagnosis," in *Proc. 6th Int. Conf. Image Signal Process. Appl. (ISPA)*, Mostaganem, Algeria, Nov. 2019, pp. 1–6.

[135] R. J. Romero-Troncoso, A. Garcia-Perez, D. Morinigo-Sotelo, O. Duque-Perez, R. A. Osornio-Rios, and M. A. Ibarra-Manzano, "Rotor unbalance and broken rotor bar detection in inverter-fed induction motors at start-up and steady-state regimes by high-resolution spectral analysis," *Electr. Power Syst. Res.*, vol. 133, pp. 142–148, Apr. 2016.

[136] T. A. Garcia-Calva, D. Morinigo-Sotelo, A. Garcia-Perez, D. Camarena-Martinez, and R. de Jesus Romero-Troncoso, "Demodulation technique for broken rotor bar detection in inverter-fed induction motor under non-stationary conditions," *IEEE Trans. Energy Convers.*, vol. 34, no. 3, pp. 1496–1503, Sep. 2019.

[137] T. A. Garcia-Calva, D. Morinigo-Sotelo, and R. de Jesus Romero-Troncoso, "Non-uniform time resampling for diagnosing broken rotor bars in inverter-fed induction motors," *IEEE Trans. Ind. Electron.*, vol. 64, no. 3, pp. 2306–2315, Mar. 2017.

[138] M. E. E.-D. Atta, D. K. Ibrahim, and M. I. Gilany, "Detection and diagnosis of bearing faults under fixed and time-varying speed conditions using persistence spectrum and multi-scale structural similarity index," *IEEE Sensors J.*, vol. 22, no. 3, pp. 2637–2646, Feb. 2022.

[139] C.-Y. Lee and T.-A. Le, "Identifying faults of rolling element based on persistence spectrum and convolutional neural network with ResNet structure," *IEEE Access*, vol. 9, pp. 78241–78252, 2021.

[140] G. Chen, M. Liu, and J. Chen, "Frequency-temporal-logic-based bearing fault diagnosis and fault interpretation using Bayesian optimization with Bayesian neural networks," *Mech. Syst. Signal Process.*, vol. 145, Nov. 2020, Art. no. 106951.

[141] W. Mao, W. Feng, Y. Liu, D. Zhang, and X. Liang, "A new deep auto-encoder method with fusing discriminant information for bearing fault diagnosis," *Mech. Syst. Signal Process.*, vol. 150, Mar. 2021, Art. no. 107233.

[142] W. Sun, S. Shaoa, R. Zhaob, R. Yana, X. Zhangc, and X. Chen, "A sparse auto-encoder-based deep neural network approach for induction motor faults classification," *Measurement*, vol. 89, pp. 171–178, Jul. 2016.

[143] F. B. Abid, M. Sallem, and A. Braham, "Robust interpretable deep learning for intelligent fault diagnosis of induction motors," *IEEE Trans. Instrum. Meas.*, vol. 69, no. 6, pp. 3506–3515, Jun. 2020.

[144] P. Kumar and A. S. Hati, "Deep convolutional neural network based on adaptive gradient optimizer for fault detection in SCIM," *ISA Trans.*, vol. 111, pp. 350–359, May 2021.

[145] A. Stief and J. Baranowski, "Fault diagnosis using interpolated kernel density estimate," *Measurement*, vol. 176, May 2021, Art. no. 109230.

[146] A. J. Skylvik, K. G. Robbersmyr, and H. V. Khang, "Data-driven fault diagnosis of induction motors using a stacked autoencoder network," in *Proc. 22nd Int. Conf. Electr. Mach. Syst. (ICEMS)*, Harbin, China, Aug. 2019, pp. 1–6.

[147] D. Xiao, C. Qin, H. Yu, Y. Huang, C. Liu, and J. Zhang, "Unsupervised machine fault diagnosis for noisy domain adaptation using marginal denoising autoencoder based on acoustic signals," *Measurement*, vol. 176, May 2021, Art. no. 109186.

[148] M. Valtierra-Rodriguez, J. R. Rivera-Guillen, J. A. Basurto-Hurtado, J. J. De-Santiago-Perez, D. Granados-Lieberman, and J. P. Amezquita-Sanchez, "Convolutional neural network and motor current signature analysis during the transient state for detection of broken rotor bars in induction motors," *Sensors*, vol. 20, no. 13, p. 3721, Jul. 2020.

[149] D. Pasqualotto, A. N. Navarro, M. Zigliotto, and J. A. Antonino-Daviu, "Automatic detection of rotor faults in induction motors by convolutional neural networks applied to stray flux signals," in *Proc. 22nd IEEE Int. Conf. Ind. Technol. (ICIT)*, vol. 1. Valencia, Spain, Mar. 2021, pp. 148–153.

[150] T. Ince, "Real-time broken rotor bar fault detection and classification by shallow 1D convolutional neural networks," *Electr. Eng.*, vol. 101, no. 2, pp. 599–608, Jun. 2019.

[151] D. Pasqualotto and M. Zigliotto, "Increasing feasibility of neural network-based early fault detection in induction motor drives," *IEEE J. Emerg. Sel. Topics Power Electron.*, vol. 10, no. 2, pp. 2042–2051, Apr. 2022.

[152] D. Reljic, D. Jerkan, and Z. Kanovic, "Broken rotor bar fault detection using advanced IM model and artificial intelligence approach," in *Proc. 18th Int. Conf. Smart Technol.*, Novi Sad, Serbia, Jul. 2019, pp. 1–6.

[153] K. Edomwandekhoe and X. Liang, "Advanced feature selection for broken rotor bar faults in induction motors," in *Proc. IEEE/IAS 54th Ind. Commercial Power Syst. Tech. Conf.*, Niagara Falls, ON, Canada, May 2018, pp. 1–10.

MOHAMED ESAM EL-DINE ATTA (Member, IEEE) received the B.S. degree in electrical power engineering from The Higher Institute of Engineering, El Shorouk Academy, Egypt, in 2010, and the M.Sc. and Ph.D. degrees in electrical power engineering from Cairo University, Cairo, Egypt, in 2015 and 2022, respectively. Since 2011, he has been with Petroleum Pipelines Company, Cairo. His research interests include power system analysis and machine fault diagnosis.

DOAA KHALIL IBRAHIM (Senior Member, IEEE) was born in Egypt, in December 1973. She received the M.Sc. and Ph.D. degrees in digital protection from Cairo University, Cairo, Egypt, in 2001 and 2005, respectively.

From 1996 to 2005, she was a Demonstrator and a Research Assistant at Cairo University, where she became an Assistant Professor in 2005, an Associate Professor in 2011, and a Professor in December 2016. From 2005 to 2008, she contributed to the World Bank Project at Higher Education Development, Egypt. From January 2010 to June 2013, she contributed as an Expert at the Program of Continuous Improvement and Qualifying for Accreditation in Higher Education, Egypt. From July 2013 to November 2014, she contributed as an Expert at the technical office of the Project Management Unit (PMU), Ministry of Higher Education, Egypt. Her research interests include digital protection of power systems, utilization and generation of electric power, distributed generation, and renewable energy sources.

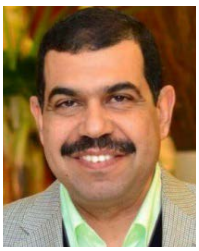

MAHMOUD I. GILANY received the B.S. and M.S. degrees in electrical power engineering from Cairo University, Egypt, in 1987 and 1989, respectively, and the Ph.D. degree in electrical power engineering from the University of Calgary, AB, Canada, in 1993. Since 1993, he has been a Faculty Member with the Faculty of Engineering, Cairo University. His research interests include power system protection, power quality, and smart networks.